TORSION BAR DESIGN FOR A FORMULA STUDENT VEHICLE SUSPENSION

JIRAPAT POTIVACHIRATORN

A THESIS REPORT SUBMITTED IN PARTIAL FULFILLMENT
OF THE REQUIMENTS FOR THE DEGREE OF
BACHELOR OF MECHANICAL ENGINEERING
SCHOOL OF INTERNATIONAL DISCIPLINARY ENGINEERING
PROGRAMS, SCHOOL OF ENGINEERING
KING MONGKUT'S INSTITUTE OF TECHNOLOGY LADKRABANG
2023

THESIS PROJECT OF YEAR 2023

MECHANICAL ENGINEERING, SCHOOL OF INTERNATIONAL

DISCIPLINARY ENGINEERING PROGRAMS, SCHOOL OF ENGINEERING

KING MONGKUT'S INSTITUTE OF TECHNOLOGY LADKRABANG

Project Title TORSION BAR DESIGN FOR A FORMULA STUDENT VEHICLE SUSPENSION

Student Name

1. Jirapat Potivachiratorn Student ID 63011158

Advisor

(Asst.Prof. Dr.Chinda Chanroenphonphanich)

TORSION BAR DESIGN FOR A FORMULA STUDENT VEHICLE SUSPENSION

Jirapat Potivachiratorn Student ID 63011158

Advisor Asst.Prof.Dr.Chinda Chanroenphonphanich

Academic year 2023

ABSTRACT

This study optimizes the torsion bar suspension systems used in Formula Student race cars. The research employs theoretical analysis, computer simulations, and experimental testing to compare materials, performance outcomes, and cost-effectiveness. The thesis emphasizes the importance of material selection in achieving a balance between performance, weight, and affordability. AISI 6150 steel is identified as a cost-effective option, while Titanium Beta C is recognized for its superior strength-to-weight ratio. The study recommends replacing coil springs with torsion bars to reduce vehicle weight and enhance overall performance. The findings indicate that material selection is crucial in balancing performance and weight while maintaining affordability. The research suggests that transitioning from coil springs to torsion bars is a strategic approach to reduce vehicle suspension weight ranging from 49% up to 65% depend on the material selection and improve overall performance.

Keywords: Torsion spring design, Spring rate, Stress analysis, Formula FSAE

, Finite element method

ACKNOWLEDGEMENT

In this thesis, I would like to express my deepest gratitude to my assistant professor of this project, Asst. Prof. Dr. Chinda Chanroenphonphanich, for sharing his expertise, guidance, and support throughout the course of my project. Without constructive feedback and his view from other perspectives, I would not have been able to complete this project effectively. I am truly grateful for the opportunity to work under his mentorship and for his positive impact on my academic journey.

Moreover, I would like to extend my thanks to Mr. Thinnakorn Kesornthong, professors, friends, and seniors who helped to properly guide me along this journey, as well as King Mongkut's Institute of Technology Ladkrabang, which provided support and resources for this project.

Lastly, I would like to thank my family, who gave me an opportunity to support me throughout the courses.

Jirapat Potivachiratorn

TABLE OF CONTENTS

Chapter. **Page**

LIST OF TABLES

LIST OF FIGURES

LIST OF SYMBOLS

W = Weight, kg or lbs.

L = Length, m

f = Force, N

T = Torque or moment (M), Nm

S = Rectilinear spring rate, N/mm or lb/in

X = Spring displacement, mm or inch

R = Length of the lever arm, m or inch

c = Radius of a shaft, m or inch

d = diameter, m or inch

ρ = Distance from the axis of the shaft to that point, m

ϕ = Angle of twist, rad

° = Degree

γ = Shear strain

γ_{max} = Maximum shearing strain

τ = Shearing stress, Pa

τ_{max} = Maximum shearing stress, Pa

G = Modulus of rigidity or shear modulus of the material, Pa

J = Polar moment of inertia, m^4

S_y = Yield strength, Pa

S_{sy} = Shear yield strength, Pa

L_a = Active length, mm

L_{oa} = Overall length, mm

L_{end} = End section length, mm

l = Transition length, mm

l_e = Equivalent length., mm

θ_{Taper} = Windup angle for a transition section with a uniform taper, rad

θ_{Arc} = Windup angle for a transition section as a circular arc, rad

M_{oa} = Overall vehicle mass, kg or lbs.

$\frac{W_f}{W_r}$ = Mass distribution related to front/ rear axis.

M_F = Overall mass on front axis, kg or lbs.

M_R = Overall mass on rear axis, kg or lbs.

M_{uF} = Overall unsprung mass on front axis, kg or lbs.

M_{uR} = Overall unsprung mass on rear axis, kg or lbs.

M_{sF} = Overall sprung mass on front axis, kg or lbs.

M_{sR} = Overall sprung mass on rear axis, kg or lbs.

K_{rF} = Front ride rate, N/m

K_{rR} = Rear ride rate, N/m

K_T = Tire spring rate, N/m

K_{wF} = Front wheel rate, N/m

K_{wR} = Rear wheel rate, N/m

CHAPTER 1

INTRODUCTION

1.1 Research Background

In 1981, the Society of Automotive Engineers (SAE) started the Formula SAE competition in the USA. That first time, only four competitor teams participated in these competitions. It became an official competition in 1982 hosted by the University of Texas. Then, it expanded to the UK and Europe in 1998; this time, the formula student became reputable as it fully progressed after that event. Nowadays, Formula Students become crucial platforms for research and development and to show a talent for engineering skills when working in the automotive industry, for example, formula 1. There are competitions worldwide, including in the USA, Germany, the UK, Australia, Japan, and Thailand.

Suspension is one of the main systems of vehicles. These systems involve tires, springs, and shock absorbers. Torsion bars are widely used, but a new concept of suspension has already been created on Formula 1 racecraft. It allows vehicle wheels to move and has supports on wheels to keep them on asphalt. A Formula Student race car is a redesigned version of an open-wheel single-seater race car, for example, F1, GP2, or the Indy 500.

Torsion bar suspension systems are vehicle suspensions that utilize the torsional resistance properties of a steel bar to provide vehicle support and damping. Unlike conventional spring-based systems, torsion bars resist the torque applied to them, twisting along their axis to absorb road impacts and smooth out the ride. This system is characterized by its simplicity, durability, and efficient use of space, making it a popular choice for many vehicles, from military tanks to commercial cars. At its core, a torsion

bar suspension includes a torsion bar anchored at one end to the vehicle's frame and connected at the other end to the wheel's suspension arm. When the wheel encounters a bump or dip, the resulting vertical movement is transferred to the torsion bar, causing it to twist. The bar's resistance to this twisting motion provides the spring action needed for the suspension system. One of the key advantages of torsion bar suspension is its adjustability; the ride height of the vehicle can be altered by adjusting the torsion bars, allowing for greater flexibility in vehicle design and performance tuning.

Moreover, torsion bar systems are known for their compactness, as the bars can be mounted longitudinally or transversely depending on the vehicle's design requirements, saving valuable space that would otherwise be occupied by bulky spring assemblies. This aspect makes it particularly beneficial for vehicles where space is at a premium, such as low-profile sports cars or heavy-duty vehicles with significant underbody armor.

Despite its many benefits, torsion bar suspension is not without its drawbacks, including potential for wear over time at the points where the bar connects to the vehicle's frame and suspension arm. Nonetheless, with proper maintenance, torsion bar systems can provide a reliable and effective suspension solution, balancing ride quality, vehicle control, and space efficiency in a wide variety of automotive applications.

1.2 Objective

1. To study structural analysis of the material when undergoes the deformation.
2. To study and design formula student suspension system to achieve the regulatory requirement of wheel travel without exceeding the strength of material.

1.3 Scope of work

1. This project focused on designing and selecting material for a torsion bar.
2. Develop a simulation to observe shear stress distribution within the bar.
3. Experiment to measure how much a material deforms under different loads and compare these results with theoretical predictions.

CHAPTER 2

LITERATURE REVIEW

Thiago Hoeltgebaum et al. [1] study offers an insightful comparison between these two types of springs, highlighting their unique characteristics, design principles, and suitability for specific applications, notably in Formula SAE cars. Coil springs, known for their wide usage in passenger cars, leverage the elastic properties of wire in torsion, providing a rectilinear spring rate ideal for independent suspensions. Torsion bars, on the other hand, employ the torsion of a steel bar to achieve a similar spring rate, offering a more straightforward, more compact design choice that has seen applications in competitive automotive fields such as Formula 1. The study adopts a detailed approach to design methodology, material selection, and fabrication processes, underpinning the decision-making process with the Pugh Matrix methodology to determine the most suitable spring type for Formula SAE applications

K. I. Ahmad et al. [2] study on applying carbon fiber-reinforced plastic (CFRP) torsion bars as an alternative to traditional grade 5 titanium alloys offers significant insights. Their research, utilizing Finite Element Analysis (FEA), demonstrates the potential advantages of CFRP in the critical suspension components of Formula 1 cars. The torsion bar, a vital element for absorbing road irregularities through its stiffness and torsional properties, is explored in this study for its performance in composite form compared to its metal alloy counterpart.

The paper presents a detailed comparison between CFRP and titanium alloy torsion bars under simulated torsional stress conditions. The findings highlight CFRP's superior stress distribution and maximum stress resistance performance, attributed to its lower density and high strength-to-weight ratio. This aligns with the overarching

goal in competitive racing to achieve lighter yet stronger vehicle components, subsequently enhancing overall racing performance.

Moreover, the study's conclusions about CFRP torsion bars offering a safer stress concentration profile and nearly half as stressed as titanium bars underscore the material's potential to revolutionize Formula 1 car suspension systems. This transition to composite materials reflects a broader trend in automotive engineering, seeking innovative solutions to improve vehicle efficiency, safety, and performance.

Zhenfeng Wang et al. [3] on the precision of torsion bar spring modeling in the pre-setting process highlights the critical role of mechanical properties, particularly elasticity, in vehicle suspension systems. Torsion bar springs, integral to the suspension, contribute significantly to a vehicle's handling, ride comfort, and overall performance. This research delves into the effects of modeling precision on the pre-setting performance of torsion bars, employing elastic-plastic theories to establish an algebraic model for analyzing stress, torque, and residual stress during the pre-setting process. Through simulations using ABAQUS software, the study reveals that torsion errors of ±1° have a negligible impact (<5%) on pre-setting performance, thus affirming the robustness of the torsion bar spring design to minor inaccuracies in torsion angle adjustments. The findings are validated against experimental data, reinforcing the conclusion that torsional performance discrepancies can be disregarded mainly within this error margin.

Julian Wisnu Wirawan et al. [4] present a detailed design analysis of the suspension system for a Formula Student race car, emphasizing the critical role of suspension in optimizing vehicle performance and handling. In the competitive realm of Formula SAE, where engineering students are tasked with designing, building, and racing small formula-style cars, the suspension system emerges as a critical factor in

achieving desired vehicle dynamics. This study focuses on an unequal double wishbone suspension system chosen for its stability at high speeds compared to other suspension types. The investigation thoroughly calculates suspension parameters to fine-tune performance, resulting in motion ratios 1:2 for the front suspension and 1:1 for the rear suspension. However, the study identifies that the front suspension's softness, attributable to spatial constraints for linkage, deviates from the optimal 1:1 motion ratio, indicating room for improvement in handling capabilities.

Ashish Vadhe's [5] study on designing and optimizing a Formula SAE suspension system provides a comprehensive examination of creating an effective suspension design for competitive racing vehicles. The research meticulously addresses the complexities of enhancing vehicle performance through the suspension system, focusing on elements such as shock absorbers, suspension travel, and the necessity for superior handling and stability. Through a combination of theoretical calculations, design parameter research, and advanced simulations using tools like ANSYS and Lotus Shark Suspension Analysis software, Vadhe explores the critical aspects of suspension geometry, including the choice of a pushrod system, and analyzes parameters like camber angle caster angle, and kingpin inclination. Additionally, the study looks into load transfer dynamics, anti-dive and anti-squat characteristics, and the significance of motion ratio and center of gravity height.

Manoj Kapoor and Kamlesh Gangrade [6] on the design and analysis of torsion bars and brackets using the Finite Element Method (FEM) provides a comprehensive insight into the optimization of suspension components for enhanced vehicle performance and safety. In their study, torsion bars, known for their critical role in absorbing road shocks and maintaining vehicle height and stability, are analyzed for

their performance under the challenging conditions of Indian roads, notorious for their roughness and unpredictability.

The study begins by highlighting the importance of torsion bars in modern Indian automotive industries, particularly in Multi-Purpose Vehicles (MPVs) and Sports Utility Vehicles (SUVs), where they are favored for their ability to be mounted low, avoiding interference with driveline components. Kapoor and Gangrade's work addresses the frequent failures of torsion bar brackets and trim height adjuster bolts under rough driving conditions, proposing design modifications to reduce the incidence of such failures.

The results revealed specific components, particularly the bolt and plate, were prone to failure under torsional loads. The assembly's resilience was significantly enhanced by upgrading material grades and increasing component thicknesses, as demonstrated by subsequent analyses that showed improved safety factors (FOS) for the modified parts.

CHAPTER 3

THEORIES AND CONCEPTS

3.1 Theories of torsion bar

The mechanical properties of a slender rod twisted around its axis are harnessed to create a rectilinear spring effect similar to that found in coil springs. The force applied to the spring is typically converted into rotational motion about the rod's central axis through a lever arm positioned at one or both ends, characteristic of anti-roll bars. Initial designs of torsion springs, such as shown in Figure 1., often assume the force acts perpendicularly to the radius throughout the twist range.

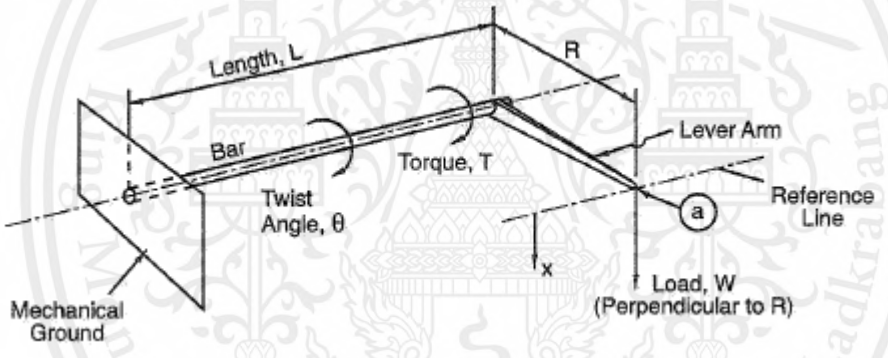

Figure 3.1 Basic geometry of a torsion spring

Source: Milliken, W. F., & Milliken, D. F. (1994). *Race Car Vehicle Dynamics*. SAE International.

However, real-world engineering requires the inclusion of correction factors for accuracy in the twist angle. The torsion bar can come in various cross-sectional profiles, from the standard circular to oval or rectangular, but in this project, we concentrate on the circular profiles. The configuration of the lever arm is not significant regarding aspects such as stress or the spring constant; its exclusive role is to transform the linear force into a moment centered on the bar's longitudinal axis. When the load is precisely

applied at point “a,” the spring’s constant is directly proportional to the rate at which the wheel responds.

3.1.1 Deformation in circular shaft

Deformation is characteristic of the circular shaft. Consider a circular shaft attached to a fixed support at one end. When torque T is exerted on its free end, the rod undergoes torsion, resulting in a rotational displacement referred to as the angle of twist, symbolized by ϕ. Within certain torque limits, this angle ϕ is directly proportional to T. Furthermore, ϕ is also directly proportional to the rod’s length L. Hence, if the rod were elongated to double its length, maintaining the same material and cross-sectional profile, the resulting twist angle would be doubled, given the identical torque T.

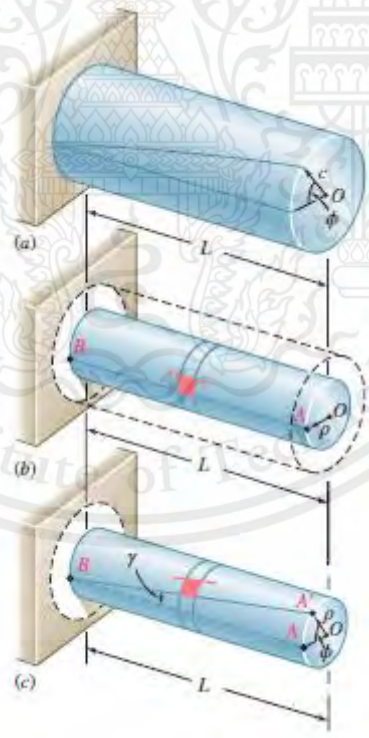

Figure 3.2 Shearing strain deformation

Source: Beer, F., Johnston, E., DeWolf, J., & Mazurek, D. (2019). *Mechanics of Materials* (8th ed.). McGraw Hill.

Initially, we trace a small square on the shaft's surface comprised of two concentric circles and two radial lines. Under torsional stress, this square deforms into a rhombus shape. The shear strain γ within a specific segment is quantified by altering the angles of the square's sides. Since the circular sides maintain their form, the shear strain γ is determined by the angle subtended by lines AB and A'B after deformation.

$$\gamma = \frac{\rho\phi}{L} \tag{3.1}$$

In this Equation, both γ and ϕ are expressed in radians, illustrating that the shearing strain at any point on a torsion shaft is directly proportional to the angle of twist. Furthermore, this relationship indicates that γ also varies in direct proportion to ρ, the radial distance from the shaft's axis to the point in question. This highlights how the degree of twist and the position within the shaft influence the extent of shear strain experienced. Based on Equation (1), it is established that the shearing strain reaches its maximum at the shaft's surface, corresponding to the location where the radius ρ equals c.

$$\gamma_{max} = \frac{c\phi}{L} \tag{3.2}$$

By removing the angle of twist ϕ from Equations (1) and (2), we can derive an expression for the shearing strain γ at a distance ρ from the shaft's axis

$$\gamma = \frac{\rho}{c}\gamma_{max} \tag{3.3}$$

3.1.2 Stress in elastic range

In the elastic range, stresses within a material follow Hooke's Law, which states that the stress experienced by a material is directly proportional to the strain applied as long as the material's elastic limit is not exceeded. This relationship ensures that the material will return to its original shape once the applied forces are removed.

For a circular shaft under torsion, the shearing stress τ at any point within the shaft can be calculated using the formula.

$$\tau = G\gamma \tag{3.4}$$

where G is the shear modulus of the material and γ is the shearing strain at that point.

$$\tau = \frac{\rho}{c}\tau_{max} \tag{3.5}$$

The radial distance ρ from the shaft's axis further defines the shearing strain, indicating that stress distribution across the shaft's cross-section is not uniform but increases linearly from the center to the outer surface.

$$\tau_{max} = \frac{Tc}{J} \tag{3.6}$$

Substitute equation (6) for equation (5). The shearing stress at any distance ρ from the axis of the shaft is determined.

$$\tau = \frac{T\rho}{J} \tag{3.7}$$

The maximum shearing stress occurs at the surface of the shaft, where the radius is most excellent. Engineers use these principles to ensure that the design of shafts and other torsional members remains within the elastic range for the expected operational loads, thereby ensuring the longevity and reliability of the components in various applications.

Additionally, when an external torque is applied to a torsion bar, the resisting moment, or the bar's ability to resist this applied torque, can be described using an alternative formula, expressed in units of lb-in, that considers the bar's cross-sectional geometry and the maximum shear stress developed within the bar.

Circular bar: $$M = \frac{\pi d^3 f}{16} \quad (3.8)$$

Square bar: $$M = d^3 f / 4.8 \quad (3.9)$$

Given that the resisting moment M matches the applied moment WR, we can express the maximum shear stress using this relationship, psi.

Circular bar: $$f = \frac{16WR}{\pi d^3} \quad (3.10)$$

Square bar: $$f = \frac{4.8WR}{d^3} \quad (3.11)$$

3.1.3 Angle of twist

The twist angle in a torsion bar, while it remains within the elastic range, refers to the rotational displacement experienced by the bar when subjected to a torque or

twisting force. This concept is crucial in understanding how materials deform under torsional stress before reaching their yield point.

In the elastic range, the twist angle is directly proportional to the applied torque and the length of the torsion bar and inversely proportional to the material's rigidity (shear modulus) and the bar's polar moment of inertia. The relationship can be mathematically expressed as this equation illustrates that the material will deform predictably under applied torque within the elastic limit but will return to its original shape once the force is removed. The polar moment of inertia is a geometric property that depends on the cross-sectional shape of the bar, with different shapes having different resistance to torsion.

$$\emptyset = \frac{\mathrm{TL}}{\mathrm{JG}} \tag{3.12}$$

Table 3.1 Polar Moment of Inertia

Geometry	Formula
Square Section	$J = \frac{a^4}{6}$
Rectangle section	$J = \frac{bd(b^2 + d^2)}{12}$
Hexagon section	$J = \frac{5\sqrt{3}}{8}s^4$
Triangle section	$J = \frac{\sqrt{3}}{48}s^4$
Circular section	$J = \frac{\pi D^4}{32}$
Tube section	$J = \frac{\pi}{32}(D^4 - d^4)$

Circle with square cutout section	$J = \frac{\pi D^4}{32} - \frac{a^4}{6}$
Circle with hexagon cutout section	$J = \frac{\pi D^4}{32} - \frac{5\sqrt{3}}{8} s^4$

Source: Polar moment of inertia for various sections. (n.d.). Retrieved from https://www.hkdivedi.com/2017/09/polar-moment-of-inertia-for-various.html

Understanding the twist angle in the elastic range is essential for designing mechanical components that can safely and reliably withstand operational stresses without undergoing permanent deformation.

3.1.4 Spring rate of torsion bar

The rectilinear spring rate, S, for a torsion bar and lever arm setup, represents the load required to achieve a linear displacement unit at the lever arm's endpoint.

$$S = \frac{W}{X} = \frac{W}{R\theta} \quad (3.13)$$

Circular bar:
$$S = \frac{0.098 d^4 G}{R^2 L} \quad (3.14)$$

Square bar:
$$S = \frac{0.141 d^4 G}{R^2 L} \quad (3.15)$$

This expression is accurate only if θ is small.

3.2 End Configuration

3.2.1 Serrate End

Serrated ends are preferred in torsion bar designs for their ability to minimize end diameters while ensuring static strength, stipulating that the minor diameter should be no less than 1.15 times the bar's diameter, according to ANSI 892.1 standards. The design process must address stress concentration at the serration root and compressive

stress on the flanks. Stress concentration occurs where the anchor meets the serration, subject to the torsion bar's torque, potentially resulting in high-stress levels. This can be mitigated by employing the largest root radius that the anchor's serration contour can accommodate, with a standard pressure angle of 45 degrees, allowing for effective shot peening. On the other hand, ensuring a large root radius can decrease the flank area, thus increasing pressure on the flanks and possibly leading to permanent deformation and fatigue fractures if not carefully managed. A balance is sought where compressive stress does not exceed 140% of the ultimate tensile stress, based on full-length contact on a portion of the serrations, calculated using Hertz's equations.

Creating serrations can precede or follow heat treatment, contingent on manufacturing preferences, although post-heat treatment serration can lead to distortions. Ensuring serrations are parallel to the bar's centerline is crucial, with shot peening adjustments to accommodate any size alterations post-machining to avoid assembly issues. Initially, serrations might not show complete contact, but the load application will establish the contact area without causing damage. Both external and internal serrations are designed to deform elastically under load, limiting contact length, with an effective serration length being 0.4 times the primary diameter to maintain integrity and functionality.

3.2.2 Hexagonal End

Hexagonal ends on round torsion bars can be created without machining, making them particularly suitable for high-volume production where upsetting machines of varying automation levels can be employed. The standard procedure involves centerless grinding of the bar stock, cutting it to the desired length, then upsetting the ends to form a hexagon shape.

This is followed by a coining operation to enhance the sides' flatness, eliminating the necessity for additional machining or grinding. Identifications such as part numbers, direction of rotation arrows, and other coded information are typically added during the upsetting process. The transition area, shaped by the material's plastic flow, remains forged. The somewhat rougher surface of this transition section is acceptable, provided there are no pits or inclusions

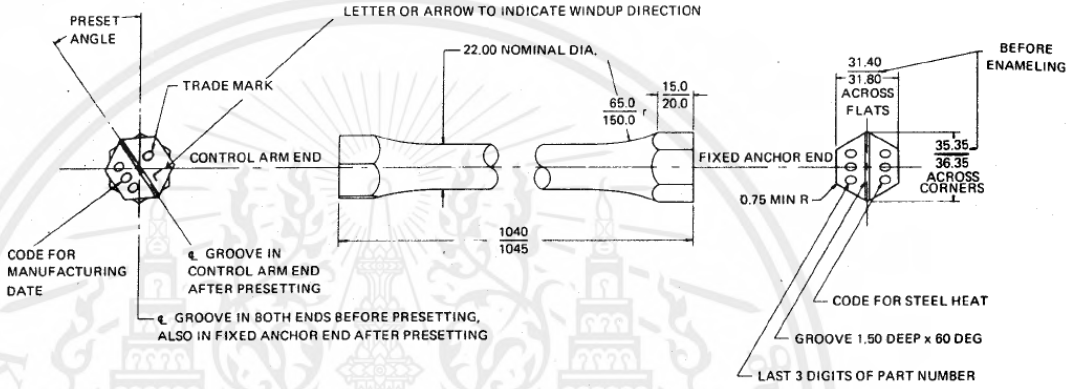

Figure 3.3 Typical design of hexagonal end configuration

Source: Manual on design and manufacture of Torsion Bar Springs: SAE HS-796. (2000). Warrendale, PA: Society of Automotive Engineers, Inc.

3.3 Anchor Member

3.3.1 Serrated Anchor Member

Stress levels within the torsion bar anchor or hub are generally lower than those in the bar itself, though areas of high local Stress levels within the torsion bar anchor or hub are generally lower than those in the bar, though areas of high local stress can occur. Internal serrations are designed with ample fillets to mitigate the risk of high-stress concentrations. Unlike other processes, shot peening is deemed unnecessary for this component. The solid design of serrations, characterized by a high-pressure angle, can lead to significant radial forces on the flanks, creating a bursting risk for the anchor

akin to the effects of internal hydraulic pressure. Ensuring the material behind the serration teeth is sufficient to counteract this internal pressure effectively.

Internal serrations are made longer than external ones for optimal engagement and to accommodate any assembly variations or tolerance issues. They are positioned to overlap with the shallow serrations at both ends. The anchor's hardness can be significantly lower than the torsion bar's, often maintained below Rockwell C 30 in many setups. Should broaching be part of the post-heat treatment process, the hardness is advised not to surpass Rockwell C 36 to preserve tool life, which aligns with ANSI B92.1 standards. This approach ensures the durability and practical function of the torsion bar system while considering manufacturing and maintenance requirements.

3.3.2 Hexagonal Anchor Member

In hexagonal anchors, similar to serrated types, areas of high stress are found, particularly at the corners of the internal hexagon. Without adequate wall thickness, these stress concentrations can lead to the anchor splitting at corners situated 180 degrees apart, especially if the torsion bar corners have excessively large radii, causing a wedging action as the bar acts like a cam.

The internal geometry of the hexagon anchor can be crafted through broaching or extruding, maintaining side parallelism within a precision of 0.004 mm per mm of length, and a surface finish finer than 1.9 μm is recommended.

The anchor's hardness should be significantly lower than that of the torsion bar to accommodate the bar's seating into the anchor faces, particularly for internal surfaces where hardness of Rockwell C 25-30 is deemed appropriate. This softer hardness allows the bar, typically in an as-forged state with a relatively rough finish, to embed slightly into the anchor, preventing the bar from resting merely on high spots, which could induce stress concentrations and lead to early failure. However, the hardness should not

drop below Rockwell C 25 to avoid excessive settling of the bar end into the anchor, which could alter the position of the anchor relative to the torsion bar significantly. The internal hexagon's length must ensure full contact between the torsion bar and the anchor, and if the anchor protrudes beyond the bar, forming a pocket, this area should be safeguarded against corrosion to prevent the retention of corrosive materials. A maximum clearance of 0.50 mm across the flats has been established to offer the necessary space between the bar and the anchor, with the minimum clearance being decided by the anchor's relative positioning and the required assembly ease.

3.4 Transition Section

To minimize stress concentrations, the transition from the bar's diameter to its end diameter should be gradual. A 30-degree included angle taper and a fillet radius 1.5 times the bar diameter is effective. Some designs prefer an arc over a uniform taper for blending the end and bar diameters, with a four times bar diameter radius proving satisfactory.

For splined torsion bars, particularly with thin-walled or tubular anchors, careful transition configurations are essential. The sharp edge at the transition radius or taper's juncture with the end diameter needs an adequate radius of three times the spline depth.

The active length (L) of a torsion bar spring, distinct from its overall length and the lengths of its end sections, includes a transition section with both inactive and active portions. The flexibility of the transition section, whether a uniform taper or arc, significantly impacts the bar's overall flexibility.

For uniform taper transitions, the equivalent length is the product of the transition length and a factor Q determined from specific diagrams. In cases of circular arc transitions, the length is derived from the bar diameter and specific factors, with the

equivalent length being the product of and another factor V, both determined from diagrams. These calculations ensure the torsion bar's performance can be accurately predicted and optimized for specific applications.

The active torsion bar spring length is The Q and V factors are calculated based on the torsional deformation experienced by a small segment of the torsion bar, characterized by length and diameter, when a torque is applied.

$$\mathrm{L} = \mathrm{L_{oa}} + 2\mathrm{L_{end}} - 2\mathrm{l} - 2\mathrm{l_e} \tag{3.16}$$

$$d\theta = \frac{32\,T\,dx}{\pi\,y^4\,G} \tag{3.17}$$

The windup angle for a section with a uniform taper can be determined through the process of integration.

$$\theta_{\mathrm{Taper}} = \frac{32\,\mathrm{TL}}{\pi \mathrm{d}^4 \mathrm{G}} \times \frac{1}{3}\left[\frac{1}{\mathrm{D}/\mathrm{d}} + \left(\frac{1}{\mathrm{D}/\mathrm{d}}\right)^2 + \left(\frac{1}{\mathrm{D}/\mathrm{d}}\right)^3\right] \tag{3.18}$$

The windup angle for a transition section shaped as a circular arc is determined through integration.

$$\theta_{Arc} = \frac{32\,TL}{\pi d^4 G} \times \frac{1}{48\left(\frac{D}{d}\right)^3}\left[8 + 10\frac{D}{d} + 15\left(\frac{D}{d}\right)^2 + 15\frac{\left(\frac{D}{d}\right)^3}{\sqrt{\frac{D}{d}-1}}\, arc\ tan\sqrt{\frac{D}{d}-1}\right] \tag{3.19}$$

This equation has been formulated for a parabolic arc instead of a circular arc to simplify the calculation process.

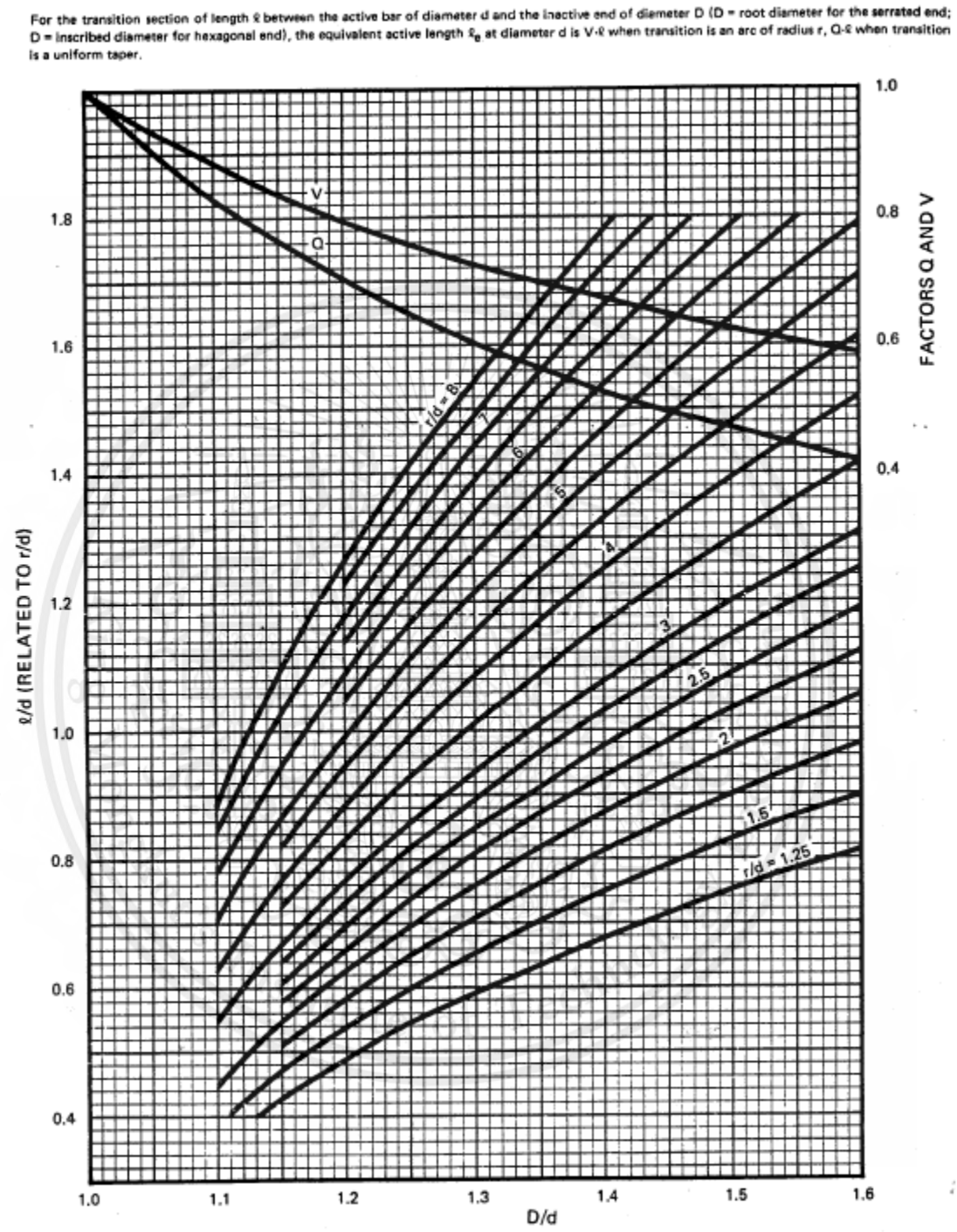

Figure 3.4 Torsion bar spring, transition data

Source: Manual on design and manufacture of Torsion Bar Springs: SAE HS-796. (2000). Warrendale, PA: Society of Automotive Engineers, Inc.

CHAPTER 4

RESEARCH METHODOLOGY

4.1 Wheel load

The load distribution across each wheel significantly influences a car's peak cornering performance in steady-state conditions. Gaining insights into the mechanics behind the development of these wheel loads can be instrumental in configuring a vehicle to achieve its optimal performance level.

A model of a quarter-sized car provides the starting point for the discussed method for determining the required suspension parameters associated with the vertical dynamics. The vehicle's mass properties provide the fundamental design parameters for the suspension provided in the table below.

Table 4.1 Vehicle mass properties

Vehicle mass properties		
Constant	Value	Unit
M_{oa}	265	Kg
$\frac{W_f}{W_r}$	47/53	
M_F	124.55	Kg
M_R	140.45	Kg
M_{uF}	30	Kg
M_{uR}	30	Kg
M_{sF}	94.55	Kg
M_{sR}	110.45	Kg

M_{oa} = overall vehicle mass.

$\frac{W_f}{W_r}$ = mass distribution related to front/ rear axis.

M_F = overall mass on front axis.

M_R = overall mass on rear axis.

M_{uF} = overall unsprung mass on front axis.

M_{uR} = overall unsprung mass on rear axis.

M_{sF} = overall sprung mass on front axis

M_{sR} = overall sprung mass on rear axis

Based on recommendations from the literature [1] for low-downforce race cars, assume front and rear ride frequency equal to, f_{nF}=2 Hz and f_{nR}=1.9 Hz. Next, the vehicle front K_{rF} and rear K_{rR} end ride rates in relation to corners express as follow.

Front ride rate:

$$K_{rF} = (2\pi f_{nF})^2 \frac{M_{sF}}{2}$$
$$= (2\pi * 2)^2 \frac{101.6}{2}$$
$$= 8026.65 \frac{N}{m} \quad (4.1)$$

Rear ride rate:

$$K_{rR} = (2\pi f_{nR})^2 \frac{M_{sR}}{2}$$
$$= (2\pi * 1.9)^2 \frac{118.4}{2} \quad (4.2)$$

$$= 8437.01 \frac{N}{m}$$

Selected spring rate K_T = 129243.61 N/m of chosen Hoosier tire 20 x 7.5 x 13 at 14 PSI

$$K_{wF,R} = \frac{K_{rF,R} K_t}{K_t - K_{rF,R}} \quad (4.3)$$

Front wheel rate:

$$K_{wF} = \frac{K_{rF} K_t}{K_t - K_{rF}}$$

$$K_{wF} = \frac{K_{rF} K_t}{K_t - K_{rF}}$$

$$K_{wF} = \frac{8026.65 \times 129243.61}{129243.61 - 8026.65}$$

$$K_{wF} = 8558.15 \frac{N}{m} \quad (4.4)$$

Rear wheel rate:

$$K_{wR} = \frac{K_{rR} K_t}{K_t - K_{rR}}$$

$$K_{wR} = \frac{8437.01 \times 129243.61}{129243.61 - 8437.01}$$

$$K_{wR} = 9026.24 \frac{N}{m} \quad (4.5)$$

In this setup, the front wheel rate is equivalent to 48.8 lb/in, while the rear wheel rate is set at 51.5 lb/in.

4.2 Motion ratio

If the spring is mounted directly to the wheel, the motion ratio is 1:1, meaning that for every inch the wheel moves, the spring compresses by an identical amount. However, in practical applications, the motion ratio often differs from 1:1 due to the suspension design and geometry. The real-world motion ratio is influenced by factors such as the placement of the spring relative to the wheel, the suspension type, and the linkage mechanisms used. These design choices affect how movement is transferred from the wheel to the spring, often resulting in a motion ratio that optimizes performance, handling, and ride comfort for specific vehicle requirements.

Similar principles regarding their behavior and analysis apply to both torsional and linear springs. Suppose the rate of a torsion bar is expressed in terms of force versus the linear displacement of its lever arm's end. In that case, the analysis mirrors that of linear springs, focusing on the effective change in spring length corresponding to the vertical displacement of the lever arm's attachment point on the suspension. However, determining the lever arm's effective installation ratio and its attachment point requires direct measurement when the torsion bar's rate is given in torque per degree (lb.-in./deg.). This process involves tracking the lever arm's angular displacement in response to variations in ride height, using an inclinometer for precision, similar to procedures used with linear springs. It's essential to measure the lever arm's angle change in a plane perpendicular to the torsion bar's axis to ensure accuracy. An approximation of the wheel rate given the torsion bar rate is as follows:

$$K_w = \frac{K_b I_B^2}{57.3} \tag{4.6}$$

We will determine the necessary spring rate to be 450 lb./in for our purposes.

4.3 Design torsion bar

SK5 metal has been chosen as the material for simulation and experimental purposes in this design approach. SK5 is a high-carbon steel known for its strength and hardness, making it an ideal choice for applications requiring durability and wear resistance. Its selection ensures consistency across simulated models and physical prototypes, facilitating accurate comparison and validation of results.

4.3.1 SK5 material properties

For this experiment, we assessed the tensile strength of SK5 steel before undergoing any heat treatment. The tensile test is carried out by affixing a strain gauge to the center of the bar, which is then connected to a data logger. This setup is designed to accurately measure the deformation of the material under applied stress, providing insight into the tensile strength of the specimen.

Figure 4.1 Data locker

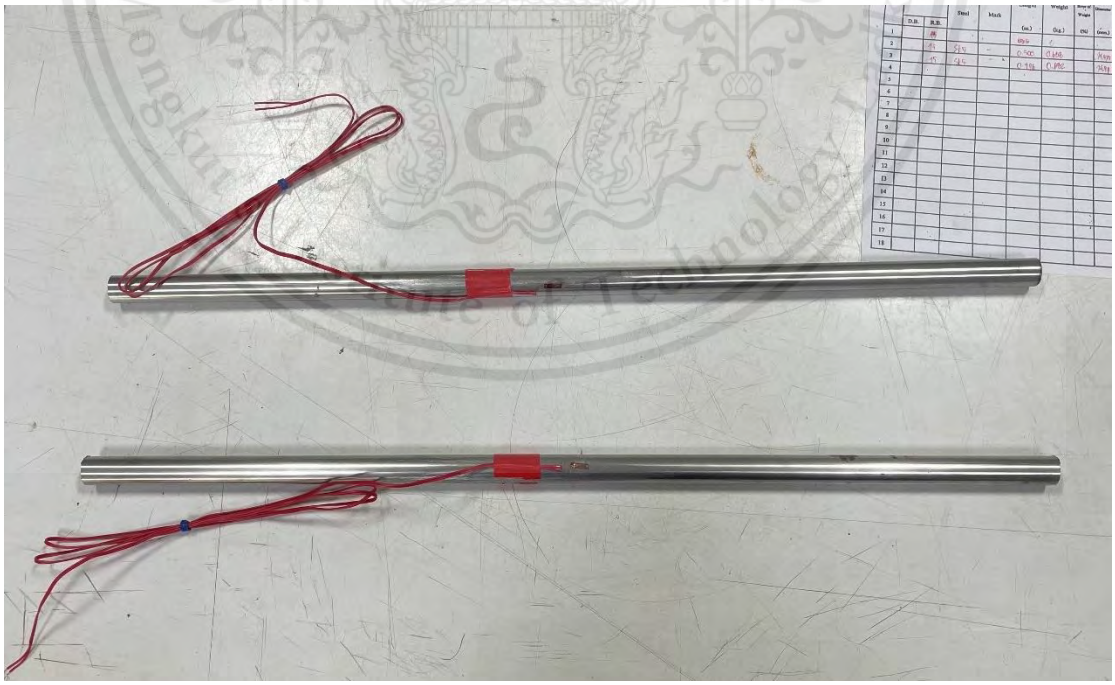

Figure 4.2 Strain gauge model: KFGS-5-120-C1-11 L1M2R

The tensile test is conducted under two distinct conditions. First, the material is gradually subjected to tension until it fails over a period of 30 minutes. This slow application of force is then compared to a more rapid test in which the material is pulled until failure within just 3 minutes. These contrasting scenarios aim to examine the effects of strain rate on the material's tensile strength and failure characteristics.

Table 4.2 Sk5 mechanical properties

Length (mm.)	Weight (Kg.)	Diameter (mm.)	Cross Sectional Area (mm.)	Load		Tensile Strength	
				Yield (Kg.)	Ultimate (Kg.)	Yield (Ksc.)	Ultimate (Ksc.)
0.500	0.688	14.975	1.761	9570.99	12997.96	5434.97	7381.01
0.496	0.682	14.99	1.764	8425.54	13886.14	4776.38	7871.96

Under the first condition, with the specimen gradually stretched to failure across 30 minutes, it exhibited a tensile yield strength of 532.96 MPa and an ultimate tensile strength of 723.83 MPa. Conversely, in the second scenario, where the specimen was quickly tensed until failure within 3 minutes, the tensile yield strength and ultimate tensile strength were measured at 468.4 MPa and 771.98 MPa, respectively.

Figure 4.3 Specimen gradually stretched to failure across 30 minutes graph

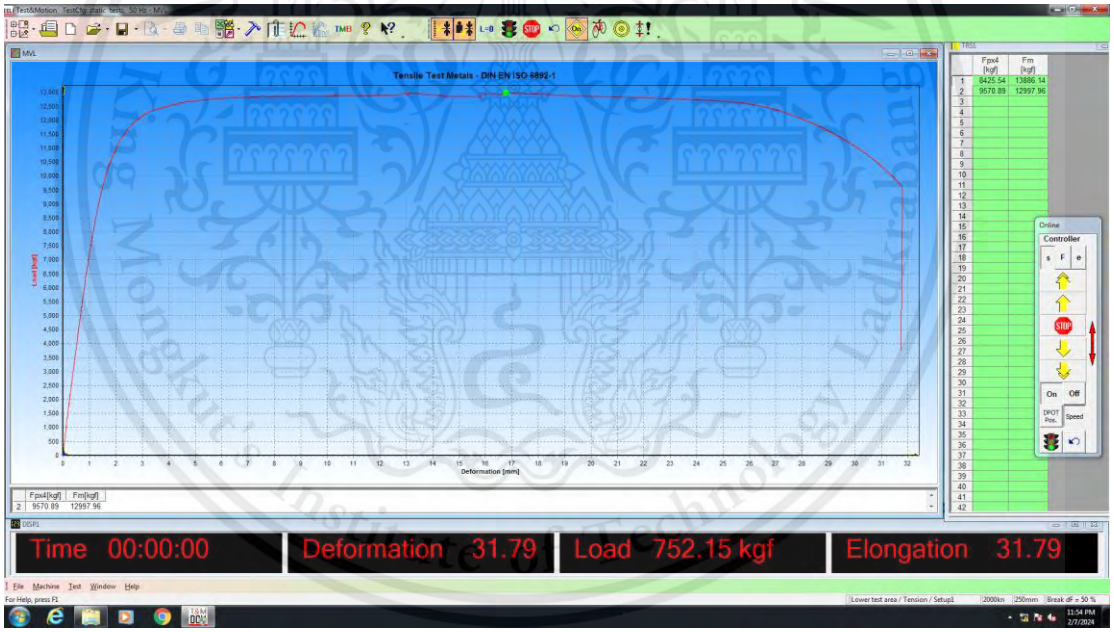

Figure 4.4 Specimen rapidly stretched to failure within 3 minutes graph

Based on the provided information, we can estimate the shear yield strength by applying the von Mises yield criterion.

$$S_{sy} = 0.577 S_y \tag{4.7}$$

Given the tensile yield strength from the first condition (532.96 MPa) and the second condition (468.4 MPa), we can calculate the shear yield strength for each condition using the von Mises criterion.

The estimated shear yield strength for the specimen in the first condition is approximately 307.70 MPa. The estimated shear yield stress in the second condition is about 270.26 MPa.

4.3.2 Design length and diameter of the bar

Given the spring rate of 450 lb/in and the shear modulus of SK5 steel at 11,603,040 psi, you can analyze the spring's behavior or dimensions using the spring rate equation (3.14).

$$S = 450 = \frac{0.098d^4G}{R^2L}$$

$$\frac{R^2L}{d^4} = 2526.884 \tag{4.8}$$

Given the estimated strength of 270.26 MPa, which is equivalent to 39,197.97 psi. Then solve with maximum stress equation (3.10). In this design, the weight of each front wheel is 47.28 kg, equivalent to 104.23 lbs. The torsion bar has been engineered to withstand three times this weight, amounting to 312.675 lbs, without experiencing failure. This design choice ensures enhanced durability and reliability under increased loads.

$$S_{sy} = \frac{16WR}{\pi d^3} \tag{4.9}$$

$$39197.9 = \frac{16 \times R \times 312.675}{\pi d^3}$$

$$\frac{R}{\pi d^3} = 7.84$$

The length of the lever arm, denoted as R, which is equal to 2 inches.

$$d^3 = \frac{2}{\pi(7.84)}$$

$$d = 0.433\ in. \quad (4.10)$$

Substitute d and R into equation (20)

$$L = 22.21\ in \quad (4.11)$$

An increase in the bar's diameter is necessary to compensate for the shortened length of the torsion bar and prevent failure due to torque load. In this specific experiment, the diameter of the bar was increased from 0.433 inches to 0.454 inches, which reduced the bar's length from 22.21 inches to 20.29 inches. Additionally, the lever arm's length significantly impacts this setup. To maintain the same spring rate despite the bar modifications, the lever arm's size was extended to 2.3 inches. This adjustment ensures that the system's performance characteristics, precisely the spring rate, remain consistent even with changes to the torsion bar's dimensions.

Figure 4.5 Torsion bar active length

4.3.3 End configuration design

In this project, a hexagonal end has been chosen over a serrated end due to its ease of machining. This decision indicates the importance of manufacturing efficiency and the practical considerations of producing components with simpler geometric shapes that still meet the required performance criteria.

Figure 4.6 End configuration design

4.3.4 Transition section design

For the transition design from the bar's diameter to its end diameter, a 30-degree included angle taper, along with a fillet radius 1.5 times the bar diameter, has been designed. This specification aligns with the recommendations outlined in reference 3,

ensuring that the design meets the required standards and recommendations.

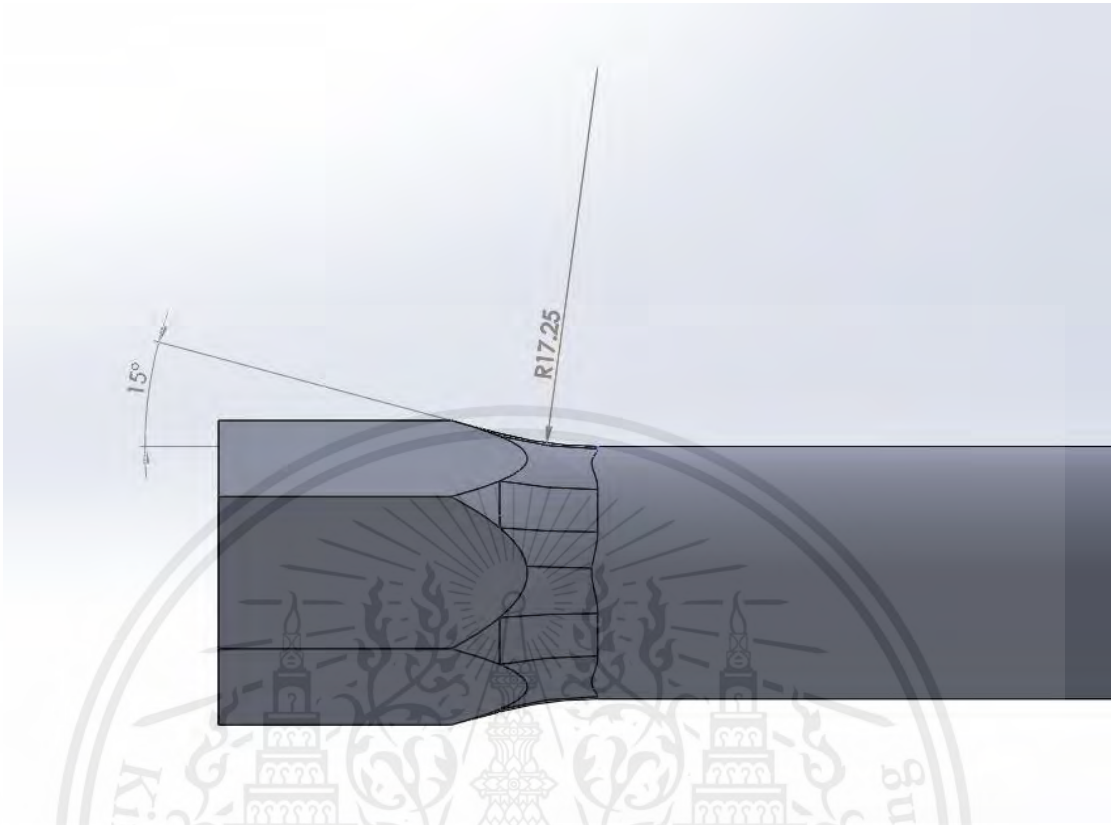

Figure 4.7 Transition section design

4.4 Material Selection

4.4.1 Titanium Beta C (Ti-3AL-8V-6Cr-4Mo-4Zr ST 815°C, Aged 425°C)

Titanium Beta C is a high-strength titanium alloy known for its excellent combination of properties, such as a high strength-to-weight ratio, outstanding corrosion resistance, and superior fatigue strength. The alloy's composition includes aluminum, vanadium, chromium, molybdenum, and zirconium, each element playing a crucial role in enhancing its overall performance. The alloy can also be heat treated to further improve its strength, with solution treatment and aging processes leading to significant gains in yield strength.

Table 4.3 Titanium Beta C mechanical properties

Constant	Value	Unit
Density	4.82	g/cc
Tensile Strength, Ultimate	1500	MPa
Tensile Strength, Yield	1420	MPa
Modulus of Elasticity	104	GPa
Poisson's ratio	0.33	
Shear modulus	40	GPa

Source: Titanium beta C (ti-3al-8v-6cr-4mo-4zr st 815°C, aged 425°C mechanical properties. (n.d.). Retrieved from https://www.matweb.com/search/datasheet.aspx?MatGUID=0cc14e76e32d407a85f224ed9b4d4bdc

4.4.2 Titanium Ti-6AL-4V (Grade 5), Annealed *(*UNS R56400*)*

Titanium Grade 5 is the most commonly used titanium alloy. Its mechanical properties and ease of fabrication have made Titanium Grade 5 a popular choice across various industries, including aerospace, medical implants, marine applications, and automotive parts. It can be heat treated for even greater strength and is known for its good weldability and machinability.

Table 4.4 Titanium T1-6AL-4V mechanical properties

Constant	Value	Unit
Density	4.43	g/cc
Tensile Strength, Ultimate	950	MPa
Tensile Strength, Yield	880	MPa
Modulus of Elasticity	113.8	GPa
Poisson's ratio	0.34	
Shear modulus	44	GPa

Source: Titanium Ti-6Al-4V (Grade 5), Annealed properties. (n.d.). Retrieved from https://asm.matweb.com/search/SpecificMaterial.asp?bassnum=mtp641

4.4.3 AISI 6150 Alloy Steel (UNS G61500)

AISI 6150 Alloy Steel is a chromium-vanadium type spring steel. It is notable for its strength, hardness, and excellent fatigue properties. The chromium content provides good hardness penetration, and the vanadium enhances the toughness and wear resistance of the steel. This combination makes AISI 6150 particularly well-suited for applications that require high fatigue strength and resistance to abrasion and impact, such as automotive parts, springs, and heavy machinery components.

Moreover, AISI 6150 can be heat-treated to achieve various strength and hardness levels, making it versatile for different engineering applications. It typically undergoes annealing, hardening, and tempering processes to optimize its mechanical properties for specific uses.

Table 4.5 AISI 6150 Alloy Steel mechanical properties

Constant	Value	Unit
Density	7.85	g/cc
Tensile Strength, Ultimate	1200	MPa
Tensile Strength, Yield	1160	MPa
Modulus of Elasticity	205	GPa
Poisson's ratio	0.29	
Shear modulus	80	GPa

Source: AISI 6150 steel, oil quenched 845°C (1550°F), 540°C (1000°F) temper, 25 mm (1 in.) round mechanicalproperties. (n.d.). Retrieved from https://www.matweb.com/search/datasheet.aspx?matguid=6fbcc44fd0124994b46587a1aa905ef0

4.4.4 AISI 5160 Steel, normalized 855°C

AISI 5160 steel is a high-carbon and chromium alloy known for its strength, durability, and excellent wear resistance. Normalizing it at 855°C (1571°F) is a heat

treatment process that improves its toughness and refines its microstructure. This treatment helps to relieve internal stresses and ensures more uniform mechanical properties throughout the material, making AISI 5160 well-suited for products like automotive springs and heavy-duty metal parts that require high tensile strength and resilience to wear and fatigue.

Table 4.6 AISI 5160 Steel mechanical properties

Constant	Value	Unit
Density	7.85	g/cc
Tensile Strength, Ultimate	958	MPa
Tensile Strength, Yield	530	MPa
Modulus of Elasticity	205	GPa
Poisson's ratio	0.29	
Shear modulus	80	GPa

Source: (N.d.). AISI 5160 steel, normalized 855°C (1570°F) properties. (n.d.). Retrieved from https://www.matweb.com/search/datasheet_print.aspx?matguid=972ec49b746d47c2a31db406e9213247

4.4.5 Material comparison

In this analysis, I will evaluate various materials for a torsion bar, maintaining the exact condition of a spring rate of 450 lb/in, similar to that of SK5. The comparison will be based on the mechanical properties of each material previously outlined.

Table 4.7 Material length comparison

Material	Length (mm)	Diameter (mm)
Sk5	510	11.5
Titanium beta C	58	8
Titanium Grade 5	122.4	9.4

AISI 6150	153	8.5
AISI 5160	434.3	11

4.5 Bell crank modification

The bell crank has undergone modifications from its original design, intended for use with coil spring suspension, to adapt it for torsion bar applications. This adaptation involves extending a hollow shaft at the pivot point of the bell crank, employing the same principles as a torsion bar. However, instead of focusing on achieving a specific spring rate, this design enhancement aims to increase torsional strength along the shaft. This enhancement is crucial for preventing potential failures due to load stresses. Additionally, the modification retains the use of the same material as the original bell crank, which is aluminum 7075. This material is chosen for its high strength-to-weight ratio, making it ideal for applications that demand durability and lightweight construction.

Figure 4.8 Original bell crank design

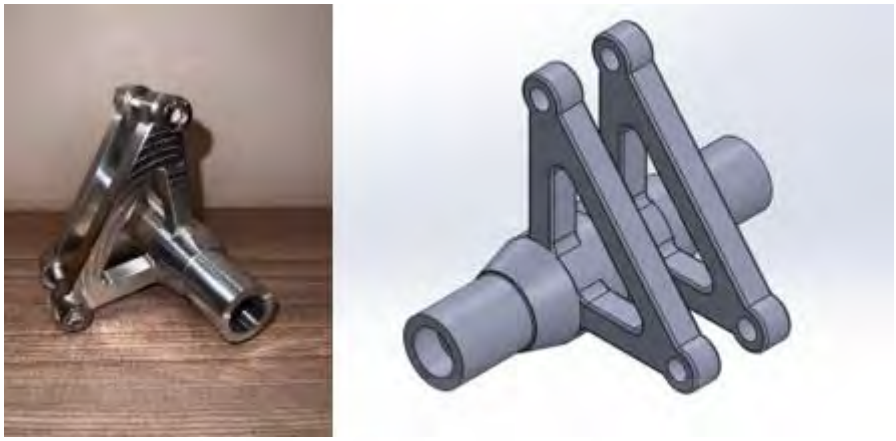

Figure 4.9 Modification bell crank design

The bearing support design in the bell crank system has been updated, shifting its position from the center of the bell crank to each end of the extended shaft. This modification enhances the support and stability of the assembly, distributing the load more evenly across the shaft and improving the system's overall response to torsional stress.

Figure 4.10 New bell crank configuration

4.6 Experimental Procedure

4.6.1 Theoretical Calculations

In this experiment, we'll assemble a simple test kit to conduct measurements and compare them against our prior calculations and simulations. The torsion bar for testing will have a length of 21.65 inches and a diameter of 0.46 inches. We plan to calculate the maximum torque this bar can handle and its twist angle.

The diameter of 0.46 inches is converted to approximately 11.6 mm, which allows us to calculate the polar moment of inertia.

$$J = \frac{\pi}{32} d^4$$

$$J = \frac{\pi}{32} (0.0116)^4$$

$$J = 1.77759 \times 10^{-9} \tag{4.12}$$

To calculate the maximum torque that a torsion bar can handle, we need to use equation (1)

$$\tau_{max} = \frac{Tc}{J}$$

$$270.26MPa = \frac{T(\frac{0.0116}{2})}{1.77759 \times 10^{-9}} \tag{4.13}$$

Solving for maximum torque equal to 82.8 Nm. Once the maximum torque that the torsion bar can withstand is identified, the maximum angle of twist can be determined using equation (1) for torsional deformation:

$$\emptyset = \frac{TL}{JG}$$

$$\emptyset_{max} = \frac{T_{max}L}{JG}$$

$$\emptyset_{max} = \frac{82.8 \times 0.550}{1.77759 \times 10^{-9} \times 80 \times 10^{9}} \quad (4.14)$$

Solving for maximum angle of twist equivalent to 0.3 rad or 17 degrees. To show how twisting changes with different forces on the torsion bar, we make a table. This table lists different forces we put on the bar and how much the bar twists for each force. It helps us see how more force leads to more twisting, up to a certain limit.

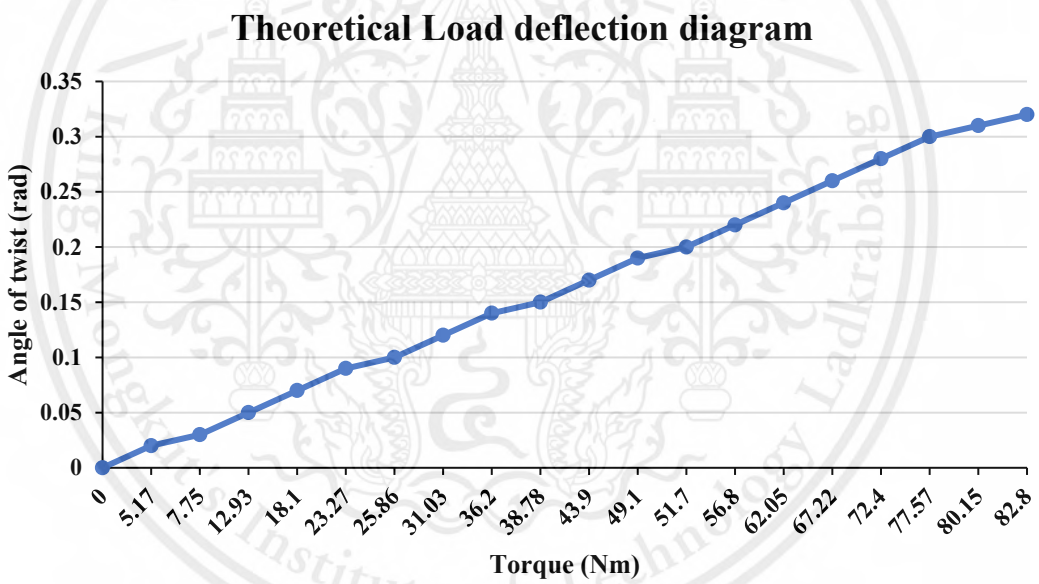

From the line graph above, the relationship between the angle of twist and the applied torque appears to be linear, suggesting that as the torque increases, the twist angle also increases at a constant rate. This is typical of elastic deformation, where the material obeys Hooke's Law up to its proportional limit.

4.6.2 Simulation Setup

In this simulation, using ANSYS for structural analysis of a torsion bar, the aim is to determine the torque that correlates with the twist angle and analyze how shear stress is distributed throughout the bar. Following this, the objective extends to comparing these findings with the results from different material bars, observing their behavior under the same boundary conditions.

Before initiating any simulation, due to the accuracy of simulation results heavily relying on the mesh quality, it's essential to conduct mesh validation first. This step ensures that the mesh, which represents the geometric space of the model, is accurate and suitable for the simulation tasks ahead. Mesh validation checks for errors or issues within the mesh that could affect the simulation's outcomes, such as inaccuracies in geometric representation, inappropriate mesh sizing, or inadequate resolution in areas of interest. Potential problems can be identified and corrected by validating the mesh beforehand, leading to more reliable and accurate simulation results.

In the process of mesh validation, assessing the mesh elements about the maximum shear stress plays a pivotal role in confirming the precision and dependability of simulations. Given the importance of shear stress in evaluating the structural strength of materials, its accurate depiction in computational models is essential. By comparing mesh elements to the peak shear stress values, it becomes possible to pinpoint sections of the mesh that require refinement to more precisely model stress distributions.

Table 4.8 Mesh validation

Element size	Element	Min	Max	Avg
2	62100	0.70458	287.19	187.42
1	494260	0.41674	294.58	184.32

0.8	958266	5.40E-03	286.22	183.81
0.6	2258348	3.13E-03	287.72	182.89
0.5	2553426	2.04E-03	293	191.52

The first step in conducting a simulation with ANSYS involves inputting the material's mechanical properties into the program. This process specifies the essential characteristics that describe how the material behaves physically, including its strength, flexibility, density, etc. This includes properties such as shear modulus, yield strength, and other relevant characteristics that influence the material's response to

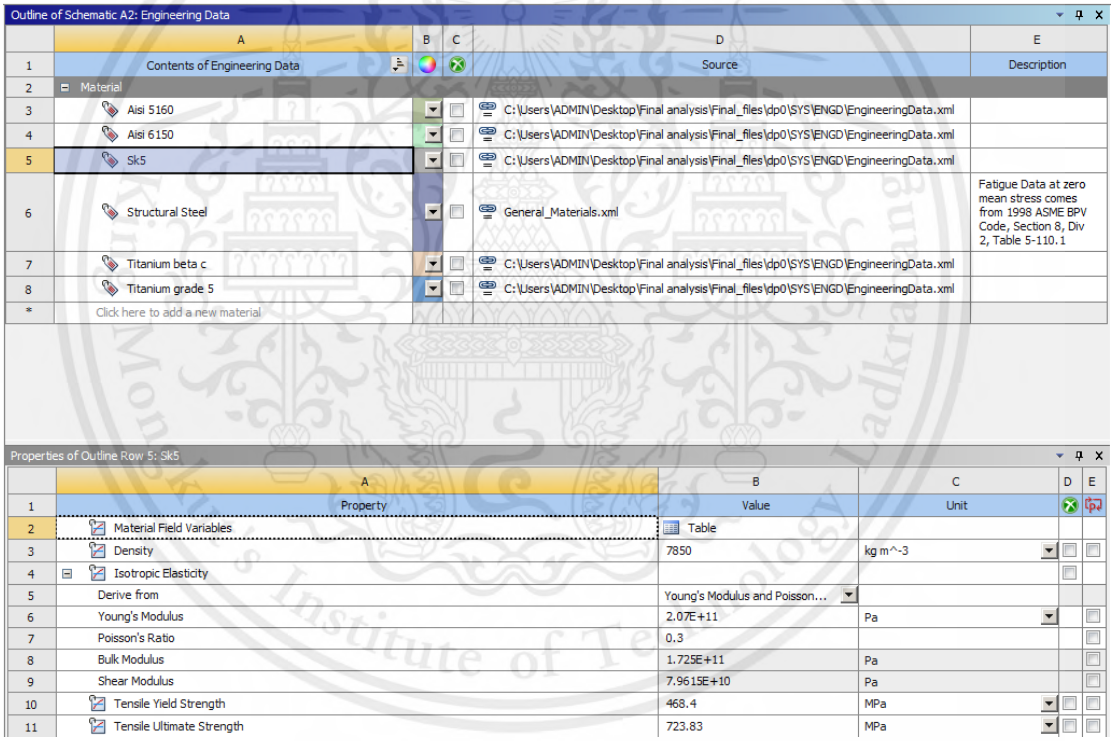

Figure 4.11 Import mechanical properties to ANSYS

Following the import of material mechanical properties, the next step involves importing the CAD model into ANSYS. This process transfers the geometric design of the torsion bar into the ANSYS, where it can be prepared for simulation.

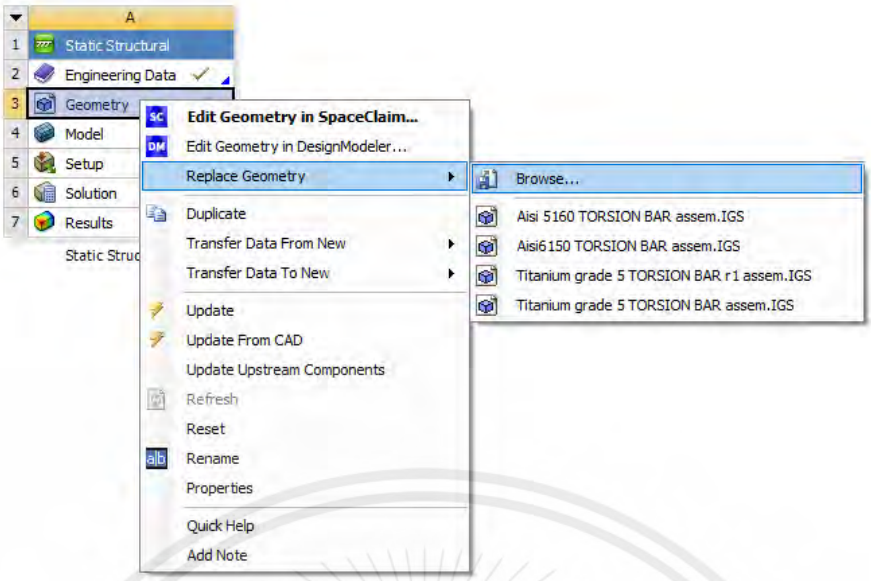

Figure 4.12 Import geometry to ANSYS

The next step involves meshing the model with an element size of 0.8mm. This site is selected to strike a balance between having a sufficiently detailed mesh to capture the necessary information and optimizing the program's processing efficiency.

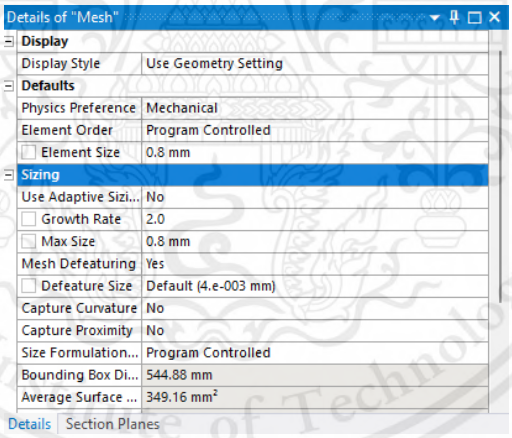

Figure 4.13 Meshing geometry

After the meshing step, the next phase involves applying boundary conditions. One end of the torsion bar is assigned a fixed support, establishing a static reference point. A remote displacement is utilized to simulate and measure the torque, allowing for the application of rotational movement and the measurement of the resultant moment. For instance, when a rotation of 1 degree is applied, the system calculates the

necessary moment to achieve that specified rotation angle at the bar's face. Finally, the simulation will be run to calculate the required moment and the distribution of shear stress along the length of the torsion bar.

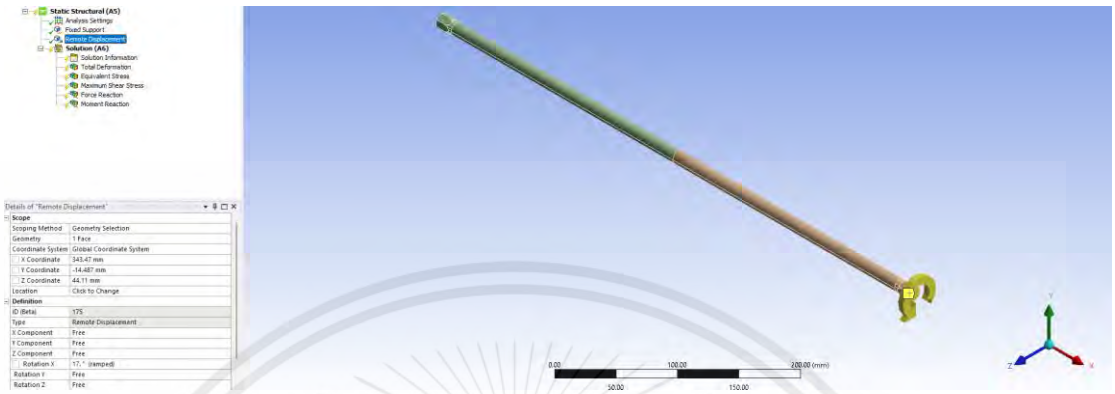

Figure 4.14 Set boundary condition

4.6.3 Experimental Setup

The experiment measures the torque needed to achieve each angle of twist, and these measurements are then compared with the predictions made based on the torsion bar's material properties and dimensions. The targeted angles of twist are carefully chosen to represent a range of working conditions for the torsion bar: 10°, 11°, and 12°, respectively.

Data will be collected using a digital torque wrench that can accurately detect and measure the amount of torque applied. The results of this experiment are critical for understanding the torsion bar's behavior under operational stresses and can provide valuable insights into the material's performance. Furthermore, the experiment is essential for confirming the torsion bar's reliability in practical applications. It is an integral part of the design and testing phase, ensuring that the torsion bar meets the required safety, durability, and performance specifications.

In the experiment's setup, one end of the torsion bar will be engaged with a torque wrench, which will apply the twisting force, while the other end will be securely fastened by a fixed support using a clamp.

This configuration ensures that the bar is immobilized at one end, providing a stable base against which the applied torques can effectively induce twist along the length of the bar. The clamp must be strong enough to resist the torques without slipping and provide accurate and consistent measurements

Figure 4.15 Experiment fixed support

Considering the torsion bar's length, it's essential to design the support system to prevent it from bending under stress. This means building a sturdy support that keeps the bar straight and correctly aligned while it's being twisted. The goal is to ensure the bar only experiences torsional forces and doesn't bend, as bending could affect the accuracy of the experiment.

Figure 4.16 Experiment shaft support

Figure 4.17 Shaft support placement

To measure the angle of the twist, I set up a reference line on a protractor, with 90 degrees as the starting point, and I marked a corresponding reference point on the torsion bar to align with this start position. Then, I carefully twisted the bar until it reached the desired target angle, ensuring measurement accuracy.

Figure 4.18 Reference point on protractor

CHAPTER 5

RESULT AND DISCUSSION

5.1 Simulation result

5.1.1 Sk5 simulation result

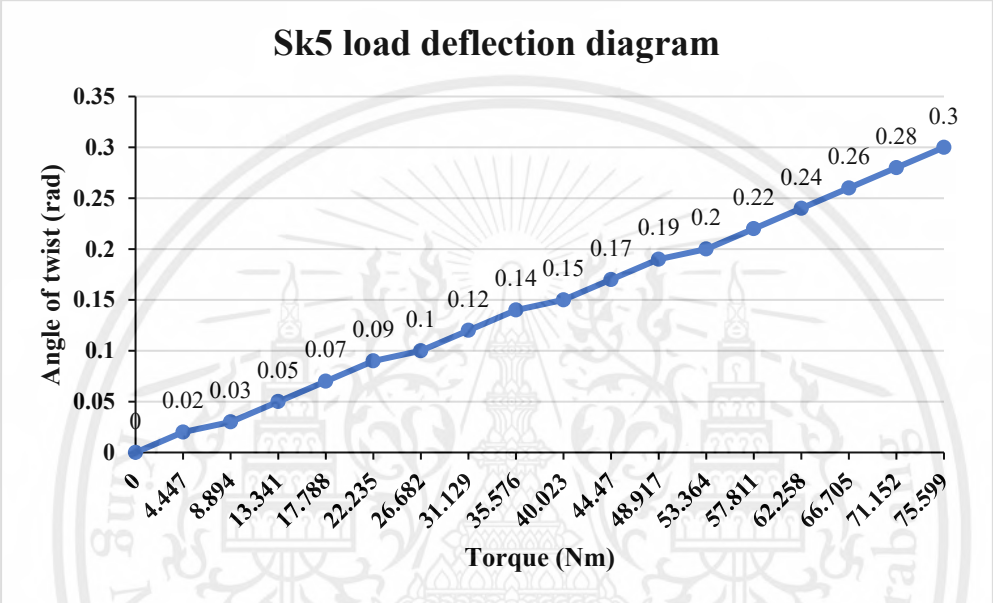

Figure 5.1 Sk5 load deflection

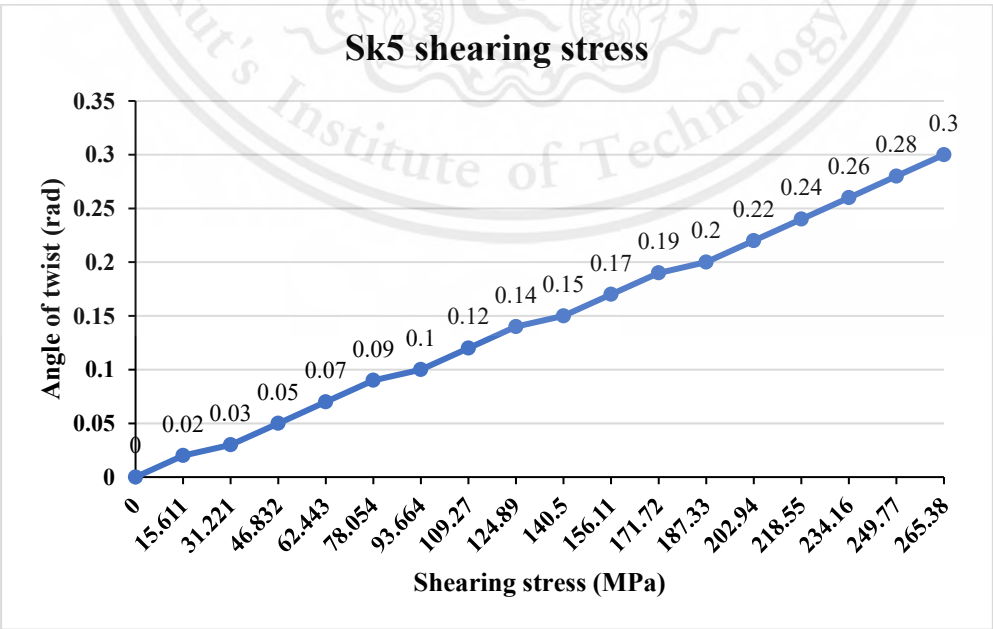

Figure 5.2 Sk5 shearing stress

Figure 5.1 shows the Sk5 load deflection diagram, which shows the relationship between torque, Nm, and angular deflection, radians. The graph shows nearly linear relationship, where the angular deflection increases as the torque increases.

Figure 5.2, Sk5 shearing stress, shows the relationship between maximum shearing stress, MPa, and angular deflection, radians. Similar to Figure 5.1, this graph shows a nearly linear relationship, indicating that the angular deflection increases as the maximum shearing stress increases.

5.1.2 Titanium beta c simulation result

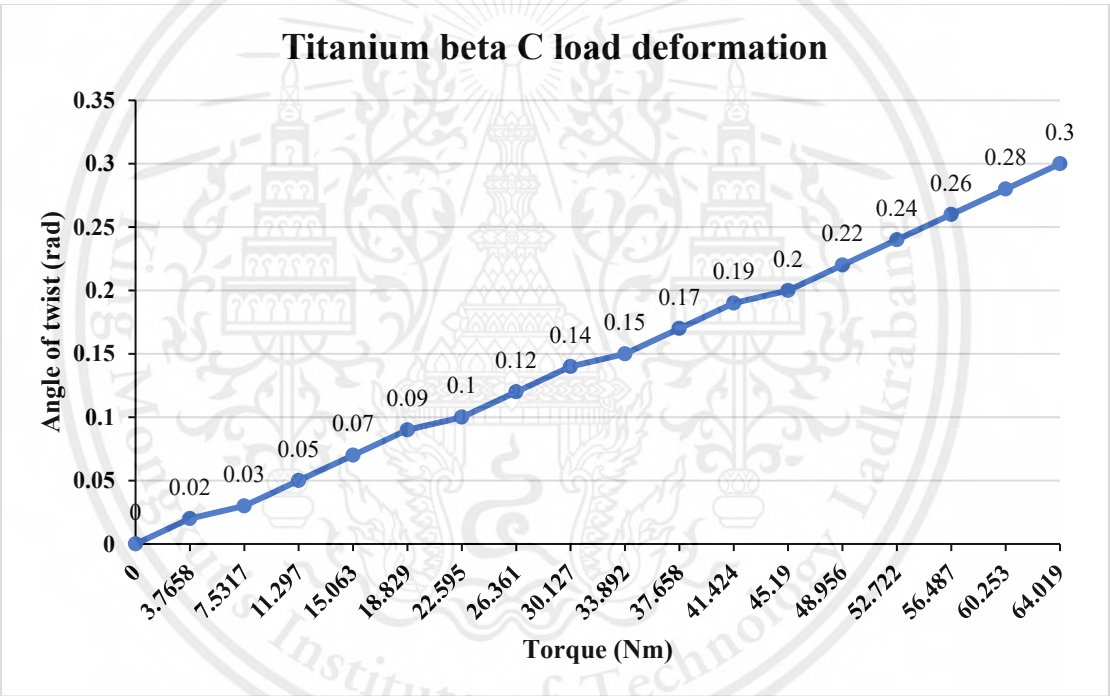

Figure 5.3 Titanium beta C load deflection

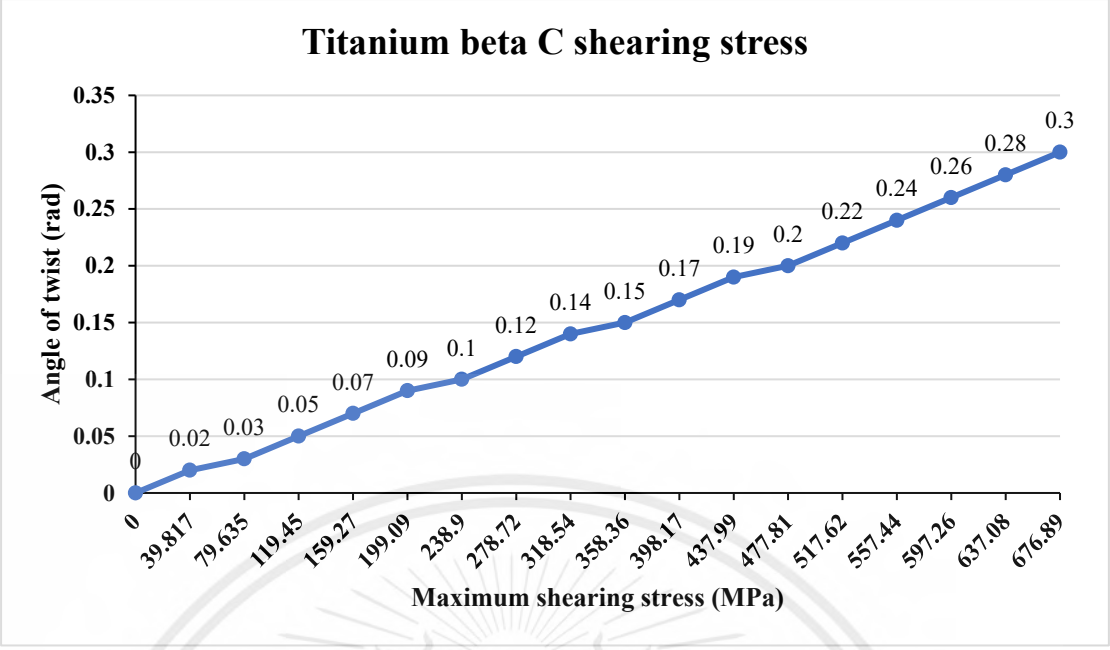

Figure 5.4 Titanium beta C shearing stress

Figure 5.3 Titanium beta C shows the relationship between torque, Nm, and angular deflection, radians. The graph also shows a nearly linear relationship, the same as Figure 5.1, under the same condition, suggesting that the materials exhibit elastic behavior within the range of the applied torque.

Figure 5.4 shares the same boundary as Figure 5.2 and shows the correlation between increasing shearing stress and the resulting increase in angular deflection. As the shearing stress escalates, so does the twist angle, implying that the material stretches elastically when subjected to torsion. This linear progression remains until the materials reach their respective yield points, beyond which they may deform permanently.

5.1.3 Titanium Grade 5 simulation result

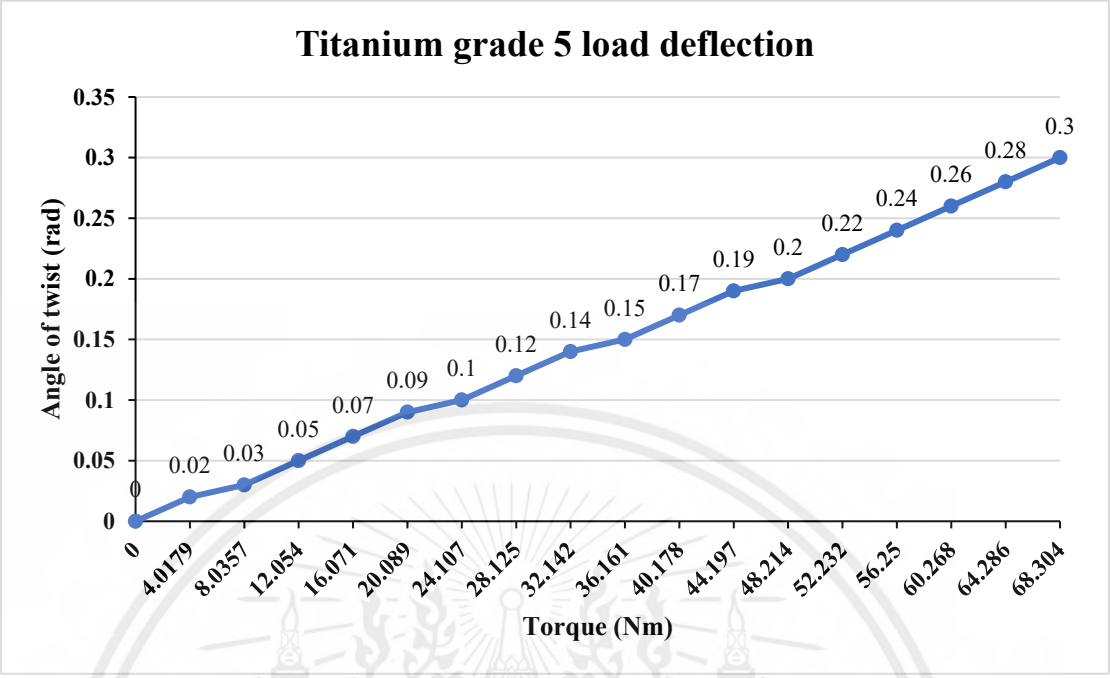

Figure 5.5 Titanium grade 5 load deflection

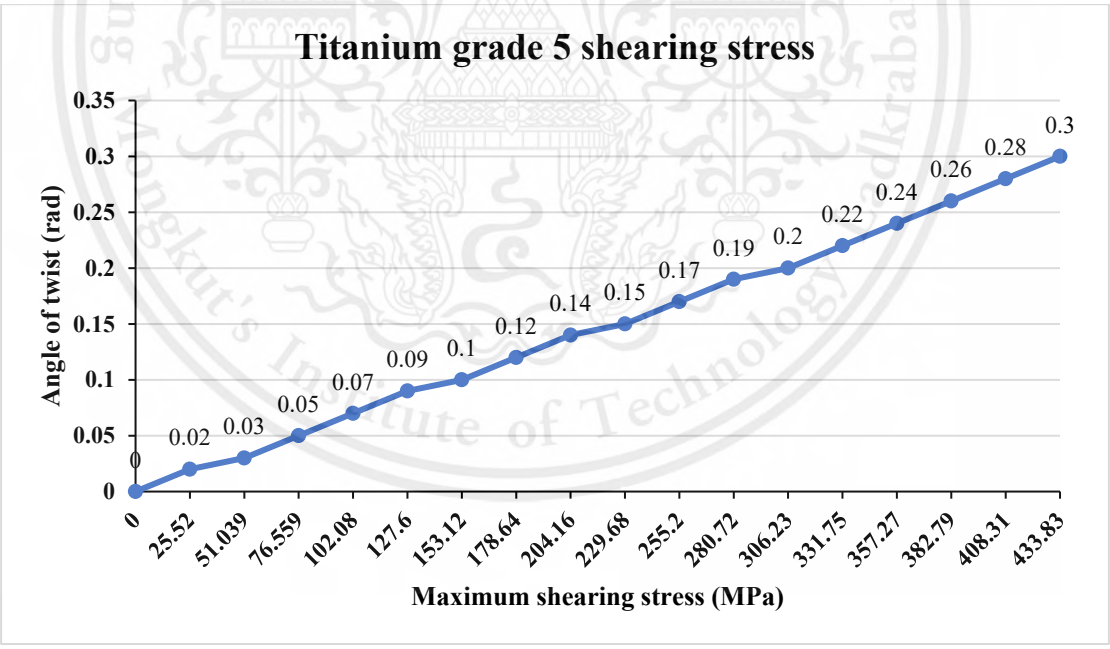

Figure 5.6 Titanium grade 5 shearing stress

Figures 5.5 and 5.6 here relate specifically to Titanium Grade 5. The graphs also show a nearly linear relationship between the applied load, torque or shear stress, and the angular deflection.

The near-linear trend in the graph suggests that within the torque range tested, the material behaves according to Hooke's Law, which states that the deformation of the material is directly proportional to the applied load, as long as the material's elastic limit is not exceeded.

5.1.4 AISI 6150 simulation result

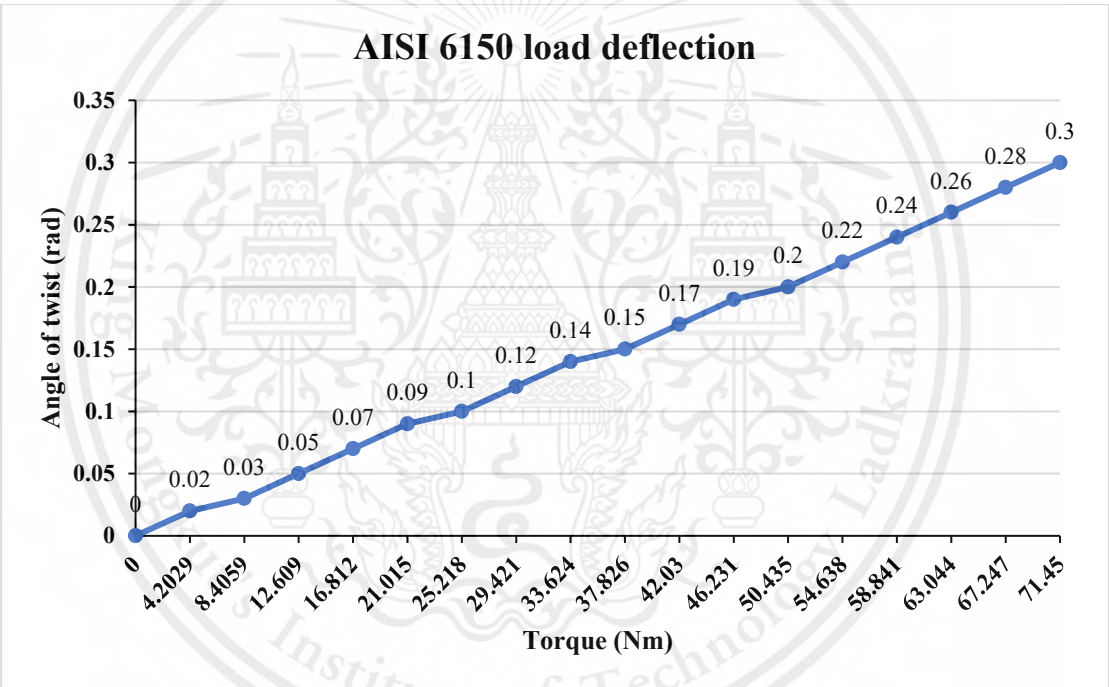

Figure 5.7 AISI 6150 load deflection

Figure 5.7, AISI 6150 load deflection, shows the elastic behavior of AISI 6150 alloy steel when a torque is applied. Each point on the line is annotated with its corresponding torque and deflection values, indicating specific measurements observed during the simulation.

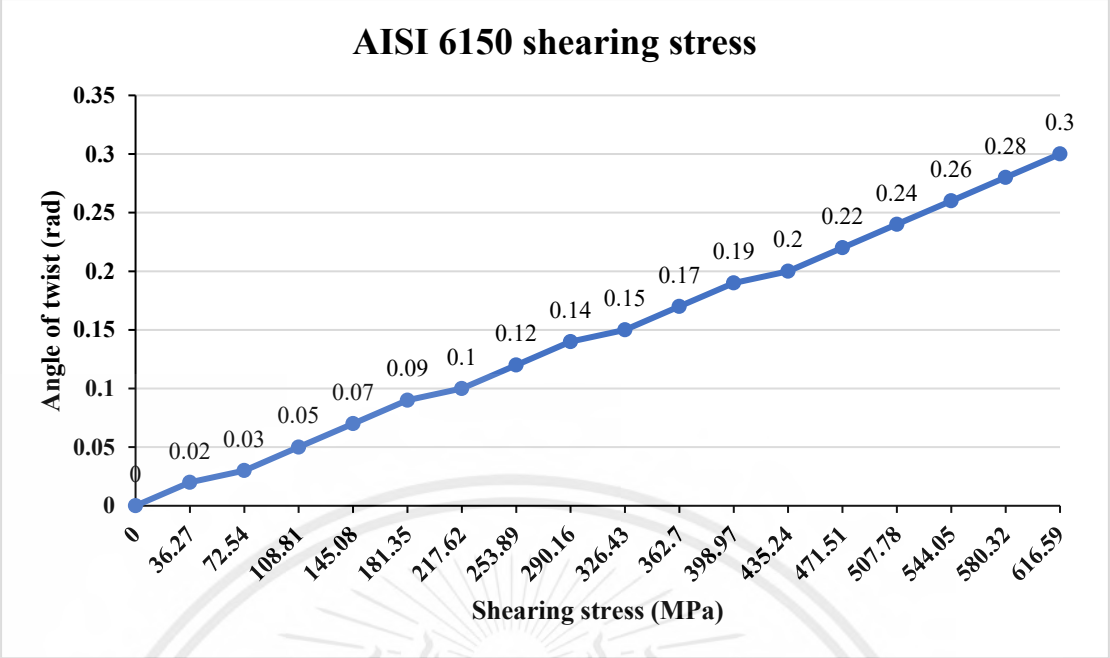

Figure 5.8 AISI 6150 shearing stress

Figure 5.8, AISI 6150 shearing stress, shows how AISI 6150 steel responds to varying levels of shearing stress in terms of angular deflection. Each point is clearly labeled with the shearing stress value and the corresponding angular deflection value.

5.1.5 AISI 5160 simulation result

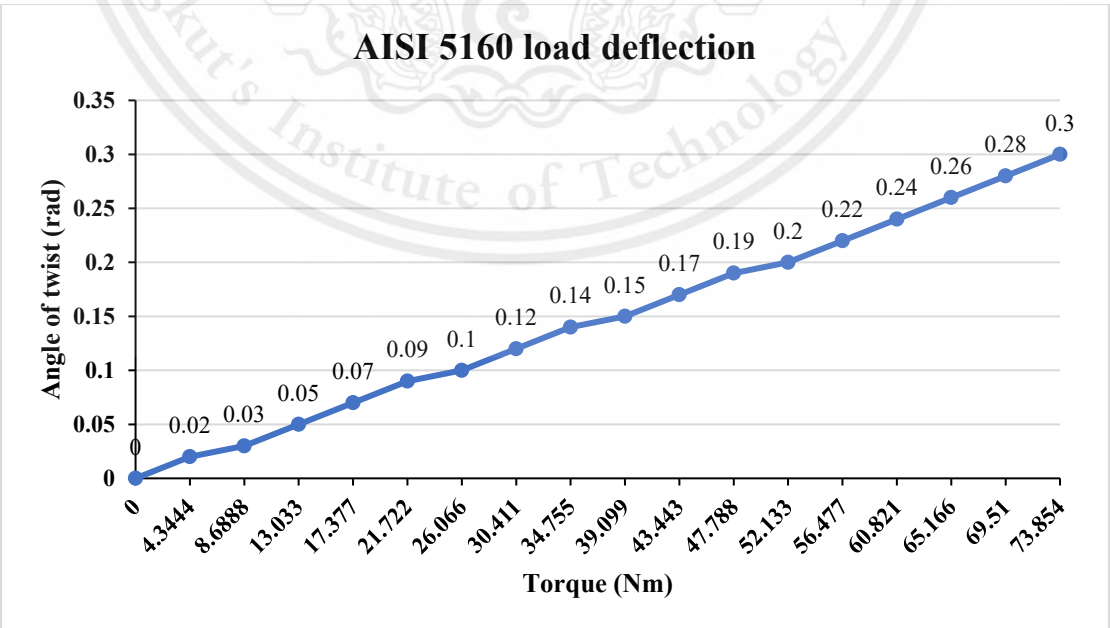

Figure 5.9 AISI 5160 load deflection

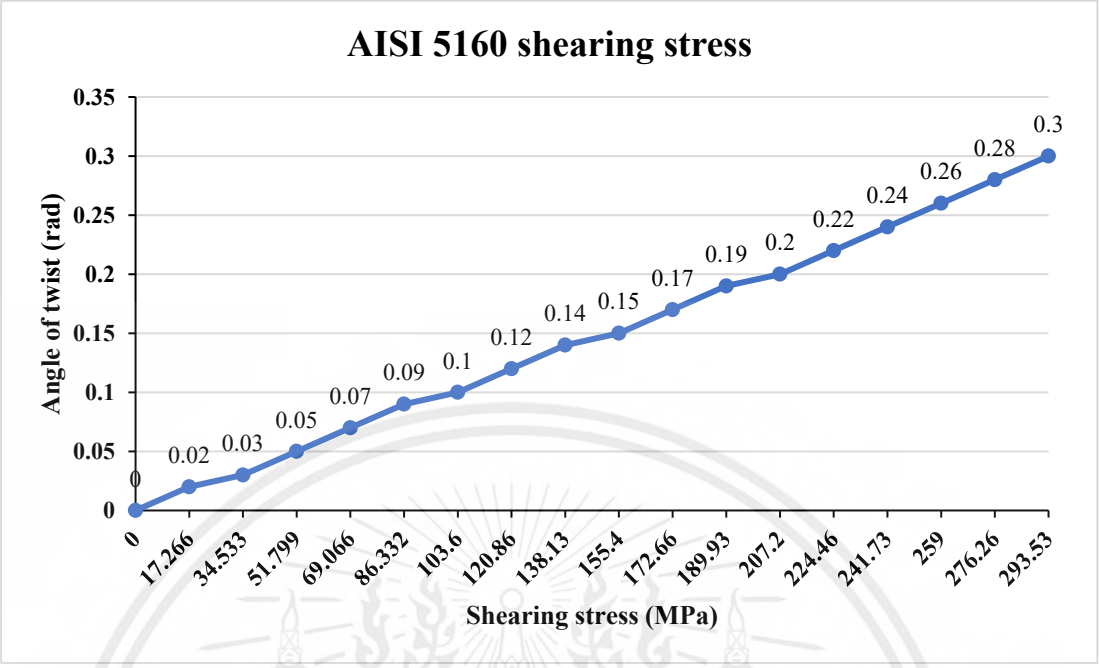

Figure 5.10 AISI 5160 shearing stress

Figure 5.9 illustrates a linear relationship between the torque applied to AISI 5160 and the angular deflection the material experiences, suggesting that the material deforms elastically within the tested range.

Figure 5.10 not only confirms our previous findings but also highlights the predictability of the material's behavior. It displays a similar linear trend, correlating the maximum shearing stress to the angular deflection. Both graphs show that as the load increases, the angular deflection increases in a predictable, and proportional manner, instilling confidence in the reliability of our results.

5.2 Experimental result

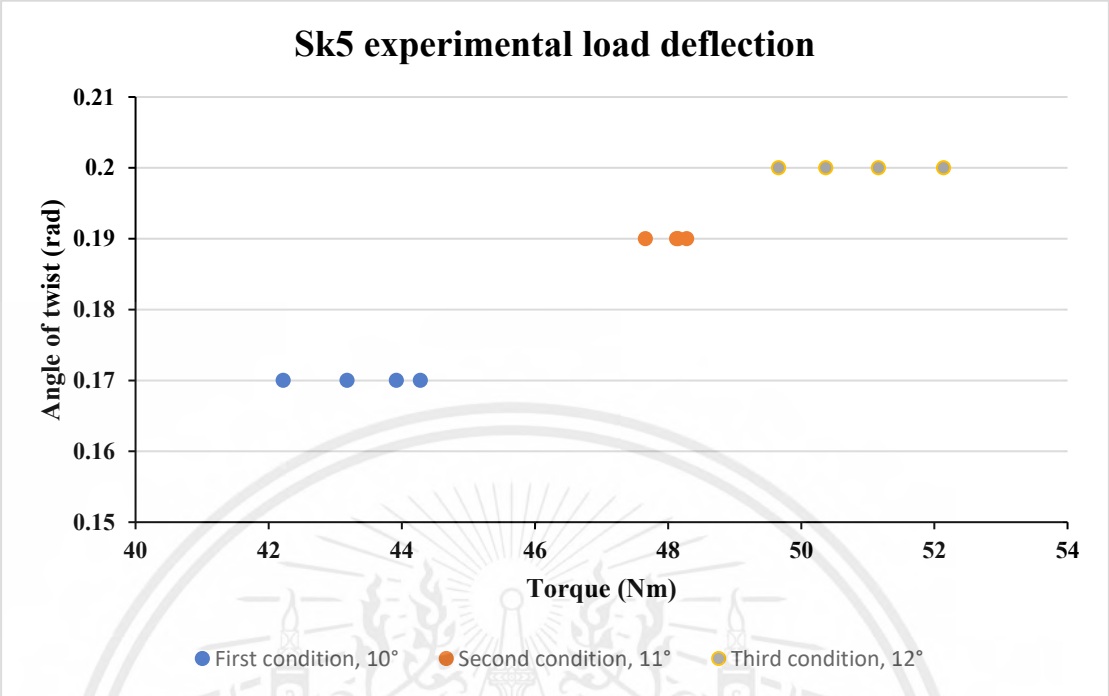

Figure 5.11 Sk5 experiment load deflection result

Figure 5.11 shows the experiment data of the correlation between the amount of torque required to achieve a specified angle of twist. Initially, to attain a twist angle of 10 degrees, the necessary torque ranged from 42 to 44 Newton meters. When the target twist angle was increased to 11 degrees, the required torque was approximately 48 Newton meters. Lastly, for a twist angle of 12 degrees, the torque needed fluctuated between 49 and 52 Newton meters.

5.3 Discussion

The outcomes obtained from both the simulation and the experimental approach can be compared against theoretical calculations. This comparison allows for a comprehensive analysis of how closely the simulation and experimental results align with theoretical expectations.

Given the potential for errors arising from limitations in the test kit, the experimental data might be subject to inaccuracies. Each condition was tested four

times to counteract this and improve the data's reliability. This method aims for the accuracy of the results by averaging across multiple trials.

Table 5.1 Result comparison between simulation, experiment, and theoretical

	Simulation	Experiment	Theoretical
First condition, 10°	44.47 Nm	43.4 Nm	43.9 Nm
Second condition, 11°	48.92 Nm	48.05 Nm	49.1 Nm
Third condition, 12°	53.36 Nm	50.83 Nm	51.7 Nm

Table 5.2 Error comparison

	Error from simulation	Error from experiment
First condition, 10°	1.3%	1.14%
Second condition, 11°	0.37%	2.14%
Third condition, 12°	3.21%	1.68%

Overall, the trend suggests the simulation is consistent but tends to underestimate the torque slightly compared to the theoretical calculations. The experimental results are generally lower than both the academic and simulation values, which could be due to experimental errors or limitations of the testing setup.

The comparison of the results from the simulation, experiment, and theoretical analysis is acceptable. However, the differences observed, particularly in the third condition, suggest it may be beneficial to re-evaluate the simulation parameters and investigate potential errors in the experimental arrangement. Furthermore, conducting multiple experiments for each condition and calculating the average of the result reduce the effects of random variations of the experimental results.

Furthermore, we will discuss the maximum shearing stress that occurs when the angle of twist reaches its peak of 17 degrees, as observed in simulation results.

Table 5.3 Factor of safety comparison

	Shear stress at 17° (MPa)	Shear yield strength of material (MPa)	Factor of safety
Sk5	265.38	270.27	1.02
Titanium beta C	676.89	819.34	1.21
Titanium grade 5	433.83	507.76	1.17
AISI 6150	616.59	669.32	1.08
AISI 5160	293.53	305.81	1.04

All of the designs tested in the simulation stay within the shear yield strength of the material, which implies that they can support a load equivalent to a quarter of the weight of a Formula Student race car, potentially up to three times that amount, without failing. Additionally, experimental observations, particularly tests involving Sk5 material, confirm following Hooke's Law. This principle states that if the material does not surpass its shear yield strength, it will return to its original shape once the applied torque is removed, indicating elastic deformation within the material's limits.

Moreover, this project's goal is to reduce weight, which is an essential consideration for a Formula Student race car, and this is a primary reason for transitioning from a coil spring configuration to a torsion bar setup. The torsion bar system offers a potential weight advantage due to its more straightforward and more compact design, contributing to the overall reduction in vehicle mass and improving the car's performance.

Table 5.4 Weight comparison

	Weight (g)	Increase/ Decrease (g)
Coil spring	400	
Sk5 Torsion bar	445.48	+45.48
Titanium beta C	36.63	-363.37
Titanium grade 5	57.98	-342.07
AISI 6150	103.89	-296.11
AISI 5160	356.16	-43.84

In my opinion, AISI 6150 steel offers a balanced compromise between cost-effectiveness in material and manufacturing and performance for creating a torsion bar. It provides the necessary mechanical properties without excessively driving up the cost. On the other hand, if the primary goal is to minimize weight drastically, then Titanium Beta C is the superior choice due to its high strength-to-weight ratio, which allows for a lighter and more compact design. Nonetheless, this advantage comes with a significantly higher cost for the material and manufacturing processes

CHAPTER 6

CONCLUSION

6.1 Conclusion

In this conclusion, the comprehensive study and experimental research on developing an effective suspension performance design for Formula Student race cars lead to significant insights into optimizing torsion bar suspension systems. This project cautiously investigates the mechanical properties, design considerations, and performance outcomes of various materials and configurations for torsion bars, aiming to enhance vehicle dynamics. The analysis reveals that material selection, Titanium Beta C, Titanium grade 5, AISI 6150 alloy steel, and AISI 5160 alloy steel plays a crucial role in balancing performance, weight, and cost-effectiveness. Furthermore, transitioning from coil springs to torsion bars is a strategic decision to reduce vehicle weight and improve overall performance. The results highlight that AISI 6150 steel is an affordable choice with good mechanical qualities; it can reduce the weight by up to 49%, including the additional weight of the modified bell crank, compared to the original coil spring suspension. At the same time, Titanium Beta C is notable for its ability to reduce weight up to 65% due to its excellent strength compared to its weight, even though it is more expensive.

6.2 Recommendation

1. It's recommended that sensors be attached during the experiment to monitor stress distribution. This will provide deeper insights, allowing for a direct comparison with theoretical calculations and simulations. Additionally, using a torsion machine to test the bar is advised, as it will yield more accurate data and minimize errors from the limitations of the testing kit.

2. For future work, it's recommended that the torsion bar system be applied to a Formula student car to observe the bar's characteristics under real conditions. This approach will enable the collection of more comprehensive data, aiding in further development of the system.

REFERENCE

[1] Hoeltgebaum, T., Luft, R. A., Elisii, J. M., & de Souza Vieira, R. (2012). A design comparison between coil springs and torsion bars. SAE Technical Paper Series. doi:10.4271/2012-36-0172

[2] Ahmad, K. I., Kariem, M. A., & Curiel-Sosa, L. (2020). T300 Carbon/Epoxy Torsion Bar as a Replacement to Grade 5 Titanium in Formula 1 Using Finite Element Analysis.

[3] Wang, Z., Dong, M., Xiang, J., Gao, P., Gu, L., & Wang, Y. (2016). Effects analysis of torsion bar spring modelling precision on properties of pre-setting process. SAE Technical Paper Series. doi:10.4271/2016-01-1327

[4] Wirawan, J. W., Ubaidillah, Aditra, R., Alnursyah, R., Rahman, R. A., & Cahyono, S. I. (2018). Design Analysis of Formula Student Race Car Suspension System. AIP Conference Proceedings. doi:10.1063/1.5024110

[5] Vadhe, A. A. (2018). Design and optimization of Formula SAE suspension system. International Journal of Current Engineering and Technology, 8(3). doi:10.14741/ijcet/v.8.3.17

[6] Kapoor, M., & Gangrade, K. (2021). International Journal of Research Publication and Reviews. Design and Analysis of Torsion Bar & Bracket Using Finite Element Method, 2(7), 762–766. doi:10.55248/gengpi

[7] Milliken, W. F., & Milliken, D. L. (1995). Race Car Vehicle Dynamics. Warrendale, Pa: Society of Automotive Engineers.

[8] Beer, F. P., DeWolf, J. T., Johnston, E. R., & Mazurek, D. F. (2020). Mechanics of Materials. New York, NY: McGraw-Hill Education.

[9] Manual on design and manufacture of Torsion Bar Springs: SAE HS-796. (2000). Warrendale, PA: Society of Automotive Engineers, Inc.

[10] Polar moment of inertia for various sections. (n.d.). Retrieved from https://www.hkdivedi.com/2017/09/polar-moment-of-inertia-for-various.html

[11] Titanium Ti-6Al-4V (Grade 5), Annealed properties. (n.d.). Retrieved from https://asm.matweb.com/search/SpecificMaterial.asp?bassnum=mtp641

[12] AISI 5160 steel, normalized 855°C (1570°F) properties. (n.d.). Retrieved from https://www.matweb.com/search/datasheet_print.aspx?matguid=972ec49b746d47c2a31db406e9213247

[13] AISI 6150 steel, oil quenched 845°C (1550°F), 540°C (1000°F) temper, 25 mm (1 in.) round mechanicalproperties. (n.d.). Retrieved from https://www.matweb.com/search/datasheet.aspx?matguid=6fbcc44fd0124994b46587a1aa905ef0

[14] Titanium beta C (ti-3al-8v-6cr-4mo-4zr st 815°C, aged 425°C mechanical properties. (n.d.). Retrieved from https://www.matweb.com/search/datasheet.aspx?MatGUID=0cc14e76e32d407a85f224ed9b4d4bdc

AUTHOR BIOGRAPHY

Author: Mr. Jirapat Potivachiratorn

Degree: Mechanical Engineering

Date: 27th October 2023

Date of Birth: 6th October 2002

Place of Birth: Bangkok, Thailand

Undergraduate and Graduate Education:

Bachelor degree in Mechanical Engineering
King Mongkut's Institute of Technology Ladkrabang Bangkok, 2024

Major: B.Eng. Mechanical Engineering